New species of mammaliaform and the cranium of *Borealestes* (Mammaliformes: Docodonta) from the Middle Jurassic of the British Isles

ELSA PANCIROLI[1,2]*, ROGER B.J. BENSON,[3] VINCENT FERNANDEZ[4,5], RICHARD J. BUTLER[6], NICHOLAS C. FRASER[1,2], ZHE-XI LUO[7] and STIG WALSH[1,2]

[1] *Natural Science Department, National Museums Scotland, Edinburgh, Scotland, EH1 1JF, UK.*

**elsa.panciroli@ed.ac.uk; nick.fraser@nms.ac.uk; s.walsh@nms.ac.uk;*

[2] *School of Geosciences, Grant Institute, University of Edinburgh, Scotland, EH9 3JW, UK.*

[3] *Department of Earth Sciences, University of Oxford, Oxford, England, OX1 3AN, UK.*

roger.benson@earth.ox.ac.uk;

[4] *European Synchrotron Radiation Facility (ESRF), Beamline ID19, Grenoble, France.*

[5] *Natural History Museum, Cromwell Road, London, UK.*

[6] *School of Geography, Earth & Environmental Sciences, University of Birmingham, Edgbaston, Birmingham, B15 2TT, UK. r.butler.1@bham.ac.uk*

[7] *Department of Organismal Biology and Anatomy, The University of Chicago, Chicago, Illinois, USA. zxluo@uchicago.edu.*

Running title: New mammaliaform and the cranium of *Borealestes*

ABSTRACT

Docodonta are one of the earliest diverging groups of mammaliaforms, and their morphology provides key information on the transition between non-mammalian cynodonts and Mammalia. We describe the partial skulls of two docodontans *Borealestes serendipitus* and ***Borealestes***

***cuillinensis* sp. nov.** from the Kilmaluag Formation (Middle Jurassic: Bathonian), Isle of Skye, Scotland. We visualize their cranial anatomy using laboratory and synchrotron X-ray micro-CT. The skulls belong to two partial skeletons, currently comprising the most complete Mesozoic mammal fossils reported from the British Isles. The associated upper and lower dentitions show that the lower dentition of *Borealestes* is not diagnostic to species level. We establish, *B. cuillinensis*, based on upper molar characters, and re-identify upper molars previously assigned to *'Borealestes' mussettae* as belonging to *B. cuillinensis*. '*Borealestes' mussettae,* based on distinctive lower molars, is found to be morphologically and phylogenetically distinct from *Borealestes*, necessitating assignment to a new genus, ***Dobunnodon* gen. nov.** The skulls of *Borealestes* retain many plesiomorphic features seen in *Morganucodon* but absent in more crownward mammaliaforms. Our study highlights that generic and species taxonomy of docodontans are more reliable when based on both upper and lower teeth, while lower molar morphology may underrepresent the true diversity of Mesozoic mammaliaforms.

Additional key words: Bathonian –Isle of Skye –Jurassic – mammals – Mesozoic – Scotland

INTRODUCTION

The early diverging mammaliaform group, Docodonta, is an extinct clade that falls outside the mammalian crown-group (Mammalia). As an outgroup to Mammalia, Docodonta can provide key information for understanding the morphological evolution of mammals as a whole (Simpson, 1929; Lillegraven & Krusat, 1991; Kielan-Jaworowska *et al., 2*004; Martin, 2018). Recent discoveries of relatively complete cranial and skeletal materials and their analyses have led to the consensus that Docodonta are closer to crown-group mammals than *Sinoconodon*

and Morganucodonta (Wible & Hopson, 1993; Luo, 1994; Luo *et al*., 2002; Martin, 2005, 2018), but probably less crownward than haramiyidans (e.g. Luo *et al*., 2015a; 2017; Zhou *et al.,* 2019). Docodonta are first known from the Middle Jurassic – when they were among the first mammaliaform clades to emerge across Eurasia (Waldman & Savage, 1972; Luo & Martin, 2007) – and become particularly abundant through the transition from the late Middle Jurassic to the Late Jurassic (Averianov & Lopatin 2006; Hu *et al*., 2006; Ji *et al.,* 2006; Averianov *et al*., 2010; Martin *et al.,* 2010; Meng *et al*., 2015; Rougier *et al*., 2015; Zhou *et al.,* 2019). The youngest docodontans currently known are *Sibirotherium* and *Khorotherium*, from the Lower Cretaceous of Russia (Maschenko *et al*., 2002; Averianov *et al*., 2018). Docodonta are hypothesized to be more closely related to the Late Triassic taxa *Tikitherium* (Datta, 2005) and *Woutersia* (Sigogneau-Russell & Hahn 1995), than to other Late Triassic mammaliaforms. If the relationships of these putative outgroups can be corroborated, Docodonta would have a long ghost lineage, extending from the Late Triassic into Middle Jurassic (Luo & Martin, 2007), although a Late Triassic split from other groups of early-diverging mammals is consistent with their hypothesized phylogenetic position.

Docodontans are unique in possessing more complex molar occluding surfaces than other early-diverging mammaliaforms, and these molar morphologies are also disparate within Docodonta (Luo & Martin, 2007). These morphologies are formed by a distinct arrangement of cusps and crests that produce crushing and shearing functions unknown in contemporary mammaliaforms, but somewhat functionally analogous to therian and australosphenidan mammals (Jenkins, 1969; Gingerich, 1973; Schultz *et al*., 2017). Docodontans also possessed some derived modern mammal-like features, such as saddle-shaped hyoids (Zhou *et al.,* 2019), and some of the intricate vascular vessels in the pars cochlearis around the inner ear (Panciroli *et al.,* 2018; Harper & Rougier 2019). However, they also retained many plesiomorphic stem mammaliaform characteristics, such as postdentary elements attached to the dentary (Lillegraven & Krusat, 1991; Ji *et al*., 2006; Meng *et al*., 2015). The discovery of more complete

skeletal material, particularly from China, has shown this group to possess an unusually wide range of locomotor specializations associated with divergent ecologies, including fossorial, semi-aquatic and arboreal specializations (Ji *et al*., 2006; Martin 2006; Luo *et al*., 2015b; Meng *et al*., 2015; Zhou *et al.,* 2019). This makes the group of key interest to our understanding of early mammal evolution.

The first docodont discovered in the British Isles was *Borealestes serendipitus*, from the Bathonian rocks of the Kilmaluag Formation near Elgol on the Isle of Skye, Scotland (Waldman & Savage, 1972) (Fig. 1). Since that time, additional teeth of *B. serendipitus* and other proposed species of *Borealestes* have been found from multiple localities of the Forest Marble Formation in England (Sigogneau-Russell, 2003; Evans, 1992). The holotype of *B. serendipitus* (BRSUG 20570) comprises part of a dentary with nine teeth (p3 to m6; Waldman & Savage, 1972; Panciroli *et al*., 2019). Much more complete fossil materials, primarily tooth-bearing mandibles, but also a partial postcranial skeleton including cranial elements (NMS G.1992.141.1 and associated material) were collected in 1973, and are now referred to *B. serendipitus* (Panciroli *et al., 2*019). A second species, '*Borealestes' mussettae*, was erected based on isolated molar teeth from penecontemporaneous sediments at Kirtlington Cement Quarry (Forest Marble Formation; Bathonian, Middle Jurassic) in Oxfordshire (Sigogneau-Russell, 2003). The taxonomic issues of *Borealestes* species were most recently examined by Panciroli *et al.* (2019).

A second partial skeleton (NMS G.2020.4.1.1) was collected from Skye in 2018, but this new find was not scanned and visualized in time for inclusion in the study of Panciroli *et al.* (2019). The new specimen reveals new diagnostic features of the upper molars that distinguish species of *Borealestes*. Specimens NMS G.1992.141.1 and NMS G.2020.4.1.1 both include associated upper and lower dentitions, including indistinguishable lower molars, but distinctly different upper molars. This observation was unexpected as it is generally assumed in studies of Mesozoic mammals that differences in upper dentitions should be reflected by differences in

lower dentitions. The upper molars of NMS G.2020.4.1.1 skeleton match those of an isolated upper molar (NHMUK PV M46871) previously referred to '*B.' mussettae* (species taxonomy *sensu* Sigogneau-Russell, 2003, interpretation by Panciroli *et al., 2*019: fig 7). The upper dentition of NMS G.2020.4.1.1, and further re-examination of taxonomic characters of the mandible allow us to establish a new species to which NHMUK PV M46871 is also referred. The holotype of '*B'. mussettae*, a lower molar with distinctively different features from the lower molars of *Borealestes* species (Panciroli *et al.*, 2019; and herein), is hereby assigned to a new genus.

MATERIAL AND METHODS

Institutional abbreviations: BRSUG (formerly UBGM), Geology Museum, University of Bristol, Bristol, UK; NMS (formerly RSM), National Museums Scotland, Chambers Street, Edinburgh, UK; NHMUK (formerly BMNH), Natural History Museum, London, UK; OUMNH, Oxford University Museum of Natural History, Oxford, UK.

Specimens

We describe the crania of NMS G.1992.47.121.1, the partial skeleton of *Borealestes serendipitus* (Fig. 2) and NMS G.2020.4.1.1, the partial skeleton of the new species *Borealestes cuillinensis* (Fig. 3). Both specimens are held in the National Museums Scotland (NMS) collections. Only the crania are described herein, the postcrania are currently under study.

NMS G.1992.47.121.1 was discovered in 1973 during fieldwork led by R. Savage and M. Waldman. A block of rock containing it was removed using a Pjonjar drill, and mechanically prepared by S. Finney at the University of Cambridge between 1994–1996 using a sodium bicarbonate airbrasive. It was then consolidated with 2% Paraloid B72. Some portions of the skeleton became detached from the limestone block (it is unclear when this occurred) and are

stored separately. These separate elements are: NMS G.1992.47.121.2, the left petrosal (Panciroli *et al.*, 2018a); NMS G.1992.47.121.3, the right dentary (Panciroli *et al.*, 2019); NMS G.1992.47.121.4, the premaxilla and nasal fragment; NMS G.1992.47.121.5 a metatarsal; NMS G.1992.47.121.6, right clavicle; NMS G.1992.47.121.7, a carpal/tarsal element; NMS G.1992.47.121.8, a chevron; NMS G.1992.47.121.9, ?cranial fragment; NMS G.1992.47.121.10, carpal/tarsal element; NMS G.1992.47.121.11, fragment of ischium; and NMS G.1992.47.121.12, fragment of rib. Only skull elements are described here.

The block containing NMS G.1992.47.121.1 was substantially larger when collected (~240 mm in length, ~170 mm in width and ~50 mm in depth) and was reduced in size by a preparator at NMS in 2015 when it became clear it required reduction to perform successful X-ray micro-computed tomography scans. All offcuts were retained. Only the section containing the skull is included herein (Fig. 2).

NMS G.2020.4.1.1 was discovered in 2018 by RJB during fieldwork by National Museums Scotland, University of Oxford and University of Birmingham. It was removed in the field using a rock saw and then reduced in size to permit µCT. Using an iterative process of pilot µCT acquisition, lossless block-splitting and removal of excess matrix using lab-based rock cutting equipment (carried out by RBJB), optimal results could be obtained without loss of fossil material. Only parts AA and BB containing the skull (Fig. 3) are included herein.

X-ray micro-computed tomography and data processing

NMS G.1992.47.121.1 was scanned at the European Synchrotron Radiation Facility (ESRF, Grenoble, France) using propagation phase contrast X-ray micro-computed tomography. The whole block was first imaged at the beamline ID17 at low resolution to locate the position of bones. The area containing skull bones was then scanned at the beamline ID19 using filtered white beam with a total integrated energy of 201 keV (wiggler 150b gap 26.5 mm; filters: Al 5.6 mm, Cu 15.6 mm, W 0.5 mm), a sample-detector propagation distance of 10 m

and an indirect detector (200 µm LuAG, 1× magnification from two Hasselblad lenses, PCO.edge 5.5) generating data with an isotropic voxel size of 6.15 µm. Each acquisition consisted of 6000 frames of 0.3 second exposure over a rotation of 360°. The centre of rotation was shifted to increase the horizontal field of view by ~85%. Several scans were needed on the vertical axis to image the full sample, keeping an overlap of ~50% between consecutive scans. Tomographic reconstruction was done using PyHST2 (Mirone *et al.,* 2014) using the single distance phase retrieval approach (Paganin *et al.,* 2002). Post processing included: modification of the bit depth from 32 bits to 16 bits, using the 0.001% minimum and maximum exclusion values of the 3D histogram generated by PyHST2; vertical stitching of the series of acquisition, using a weighted average based on the vertical intensity profile of the beam; ring correction (Lyckegaard *et al.,* 2011); cropping of the volume. Finally, we applied a binning 2×2×2 to reduce the data size while increasing the signal-to-noise ratio, making it easier to segment the data.

Other specimens were imaged using laboratory X-ray µCT at various facilities (parameters for each acquisition are listed in Table 1). NMS G.1992.47.121.2 and NMS G.1992.47.121.4 were scanned at the University of Edinburgh by I. Butler and EP at the School of Geosciences Experimental Geoscience Facility, using their in-house built µCT system. The system comprises a Feinfocus 10-160 kV dual transmission/reflection source (Feinfocus Röntgen-Systeme GmbH, Garbsen, Germany), MICOS UPR-160-AIR ultra-high precision air-bearing table (PI miCos GmbH, Eschbach, Germany), Perkin Elmer XRD0822 amorphous silicon x-ray flat panel detector and terbium doped gadolinium oxy-sulfide scintillator (PerkinElmer, Waltham, USA). Data acquisition software was written in-house, and tomographic reconstruction were performed by I. Butler using Octopus 8.7 software (TESCAN Orsay Holding a.s., Brno, Czech Republic). Data for NMS G.1992.47.121.2 have a voxel size of 8.9 µm, and for NMS G.1992.47.121.4 a voxel size of 6.43 µm.

X-ray micro-computed tomographic data for NMS G.1992.47.121.3 and all parts of NMS G.2020.4.1.1 were obtained by RBJB and T. Davies, and were imaged at the University of

Bristol using a Nikon XTH 225 ST (Nikon Metrology, Leuven, Belgium) with a 225 kV rotating target. The scan resolution for NMS G.1992.47.121.3 was 12.77 µm and for NMS G.2020.4.1.1 parts AA and BB the scan resolution was 22.14 µm and 20.05 µm respectively.

All tomographic data were segmented and digitally reconstructed by EP using Mimics 19.0 (Materialise NV, Leuven, Belgium) at NMS and the University of Oxford. Where possible (i.e. when they were not covered completely by matrix or sediment), specimens were also observed using conventional microscopy at NMS. Measurements were taken using the measurement tools in Mimics 19.0, and corroborated with manual measurements using fine callipers or a microscope where possible. Tooth measurement methodology and cusp nomenclature are as in Panciroli *et al.* (2019). CT data and resulting 3D models are available at Morphosource (www.morphosource.org/Detail/ProjectDetail/Show/project_id/1092).

Phylogenetic analysis

We analysed the character matrix of Panciroli *et al.* (2019), modified from Meng *et al*. (2015), with the addition of characters states for *B. cuillinensis*, and revising character states for '*B.' mussettae*. This data matrix has 25 taxa, scored for 48 characters of the dentary and dentition only (characters of the crania and postcrania are currently being scored for a larger phylogenetic analysis in progress). We analysed these data using PAUP*4.0 Version 4 (Swofford, 2003), conducting a branch-and-bound tree search using parsimony with characters unordered and equally weighted. Six equally most parsimonious trees of 131 steps were retained, and summarized as a strict consensus tree, scaled to time using data from Panciroli *et al*. (2019). Full datasets and details of analysis can be found in Supplementary Material.

Geological background

Specimens described herein (except NHMUK PV M46495) were collected from the Kilmaluag Formation (Harris & Hudson, 1980) on the Strathaird Peninsula of the Isle of Skye (Fig. 1). The

Kilmaluag Formation is part of the Great Estuarine Group (formerly Great Estuarine Series [Judd 1878: 722]). This formation comprises a series of near-shore shallow marine, varied salinity lagoon and freshwater lagoon sediments of Bathonian age (Harris & Hudson, 1980; Andrews, 1985; Barron *et al.,* 2012). These Mesozoic sediments are overlain disconformably by Cenozoic basalt (Harris & Hudson, 1980).

The Kilmaluag Formation crops out on the islands of Eigg, Skye and Muck, in the Inner Hebrides of Scotland. It is approximately 25 m in thickness at the most complete section on the Strathaird Peninsula, where there are predominantly argillaceous (muddy) limestone facies (Harris & Hudson, 1980; Andrews, 1985; Morton & Hudson, 1985). The Kilmaluag Formation falls within the *Retrocostatum* Zone, of Late Bathonian age (Barron *et al.,* 2012), just over 166.1 Mya (Cohen *et al.,* 2019). It includes predominantly low-salinity and freshwater facies, especially on the Strathaird Peninsula, as demonstrated by the presence of freshwater ostracods *Darwinula* and *Theriosynoecum* (Wakefield, 1995), shallow freshwater to oligohaline conchostracans such as *Antronestheria* and *Pseudograpta* (Chen & Hudson, 1991) and freshwater gastropods *Viviparus* (Andrews, 1985; Morton & Hudson, 1995; Barron *et al.,* 2012).

Vertebrate fossils are thought to predominantly come from the 'Vertebrate Beds', horizons 9 and 10 of Andrews (1985). These beds alternate between muddy carbonates, hard blue-grey limestones, micrites, wackestones and breccia conglomerates, and appear to be predominantly freshwater in origin (Andrews, 1985). Vertebrate fossils from multiple groups have been found in these beds (Evans *et al.,* 2006; Panciroli *et al*., 2020), including fish (Rees & Underwood, 2006), amphibians (Evans & Waldman, 1996), lepidosaurs (Waldman & Evans, 1994; Evans & Waldman, 1996), testudines (Anquetin *et al., 2*009, 2010) mammaliamorphs and mammaliaforms (Waldman & Savage, 1972; Close *et al*., 2016; Panciroli *et al*., 2017a, b, 2018b), crocodylomorphs (Wills *et al*., 2014) and dinosaurs (Barrett 2006). NMS G.2020.4.1.1 was collected from the top of a 1 metre thick argillaceous limestone, bed 9C of Andrews (1985), close to the base of the 'Vertebrate Beds'. Vertebrate fossils (including NMS G.1992.47.121.1)

are also recovered from loose boulders on the foreshore. It is not certain which exact horizons these boulders come from, but the lithology is congruent with the 'Vertebrate Beds'.

RESULTS

Phylogenetic Analysis

The results of our phylogenetic analysis support the sister-taxon relationship of *Borealestes serendipitus* and *Borealestes cuillinensis*, and the placement of *Dobunnodon mussettae* as the sister to a clade comprising *Borealestes* species, *Docofossor*, *Docodon* and *Haldanodon* (Fig. 4). This phylogenetic result, and the morphological distinctiveness of the lower molars of *D. mussettae* indicates the need for a separate genus to accommodate the type species of '*Borealestes' mussettae*.

Relationships among the rest of Docodonta are the same as recovered in Panciroli *et al*. (2019), but there is less support for the clade Tegotheriidae (proposed by Averianov *et al*. 2010). A larger analysis incorporating cranial and postcranial characters scored from NMS G.1992.47.121.1 (and associated material) and NMS G.2020.4.1.1 is currently underway, and may add further insight into the relationships within Docodonta.

SYSTEMATIC PALAEONTOLOGY

Mammaliaformes Rowe, 1988

Docodonta Kretzoi, 1946

Docodontidae Simpson, 1929

Borealestes Waldman & Savage, 1972

Type species: Borealestes serendipitus Waldman & Savage, 1972

Revised differential diagnosis

Dental formula 4.1.?5.4/4.1.5.5(6). As in other docodontans: possesses an anterior 'pseudotalonid basin' formed by cusps a, b, and g; retains plesiomorphic mammaliaform trait of attachment of postdentary elements to the dentary; has an eflected angular process (sensu Simpson, 1929; also see Schultz *et al.,* 2017: figs. 2 and 3); enlarged medial ridge protuberance (sensu Schultz *et al*., 2017); enlarged and pointed upper and lower canines that are twin-rooted. The lower molars of *Borealestes* are: elongated anteroposteriorly, with labial row of higher cusps arranged in anteroposterior alignment with largest cusp a, and lingual row of smaller cusps with distinctive anterior cusp g and larger posterior cusp c; lower molars have cusps b–a–c in a triangular arrangement. The a–g crest on cusp a is absent (present to variable extent on cusp g) and the a–d crest on cusp a is also absent (but a labially oriented a–d crest is present on cusp d). *Borealestes* has a distinctive a–c crest. Upper molars of *Borealestes*: buccolingually wide and anteroposteriorly short; 'figure 8' shape, with anteroposteriorly constricted waist; two main buccal cusps, A and C, plus a small cusp B in the buccomesial corner; lingual half of the upper molar has main anterior lingual cusp X; cusp X larger and more prominent than smaller posterior lingual cusp Y; labial cusps connected by a ridge/ridges anteroposteriorly; transverse ridge extends between the main anterior labial cusp A and the main lingual cusp X. In the lower molars *Borealestes* most closely resembles docodontans *Krusatodon*, *Castorocauda*, and *Haldanodon* in sharing a larger cusp c than cusp g. It resembles *Castorocauda* and possibly also *Itatodon* in having a slightly recurved cusp c. *Borealestes* is similar to *Castorocauda* and *Docodon* in possessing an anterior 'cingulid' incorporating cusp e, and cusp e is anteriorly projecting and forms part of the d–df–e interlock with the neighbouring molar, as in *Krusatodon* and *Simpsonodon*. *Borealestes* has a distinct lingual cingulid in the premolars, and a posterior labial cingulid, as seen in most other docodontans. Unlike *Simpsonodon*, *Agilodocodon*, and *Docodon*, but like most other docodontans, *Borealestes* does not have dense creases and pits or other ornamentation on molar enamel surfaces. *Borealestes* differs from *Dobunnodon*

mussettae in having more elevated b-g crest and c-d crest, and the more lingually positioned cusp e. *Borealestes* differs from all other docodontans except *Docodon* in having an anterior fovea (*sensu* Panciroli *et al.,* 2019: fig 1B3) on the upper molars: a concave area anterior to the anterolingual crest. *Borealestes* differs from *Docodon* in having the anterior fovea positioned at the anteroposteriorly constricted waist of the upper molars. *Borealestes* differs from *Krusatodon*, *Agilodocodon*, *Simpsonodon*, *Docodon*, and *Haldanodon* in having transversely expanded and anteroposteriorly slightly compressed lingual wing of the upper molar, similar to *Docofossor* and *Dsungarodon*. *Borealestes* resembles *Docofossor* and *Dsungarodon* in having more reduced cusps Y and Z on the upper molars, and a larger cusp X.

Referred specimens

Specimens referred to *Borealestes* sp. but not to species level—from the Kilmaluag Formation, Isle of Skye: BRSUG 29007, fragment of right dentary; BRSUG 29008, three fragmentary molars in matrix.

BOREALESTES SERENDIPITUS Waldman & Savage, 1972

Differential diagnosis

Dental formula 4.1.?5.4/?4.1.5.5(6). *Borealestes serendipitus* differs from *Borealestes cuillinensis*, the only other species in the genus, in having distinct anterolabial and anterolingual crests between cusps A and X in the upper molars, and in that cusp Z is reduced (Figs 5 and 6). The anterior fovea is more distinct than in *B. cuillinensis*. The lower molar cusps are slightly less dorsoventrally tall in *B. serendipitus* than in *B. cuillinensis*. The lappets of the dentary enclose the cartilage of the Meckel's sulcus of *B. serendipitus* from the point ventral to the m3-m4 in adult specimens, leaving a faint line running anteriorly, unlike in *B. cuillinensis* where it remains

an open sulcus in adult (Fig. 7). The mandibular symphysis of *B. serendipitus* remains distinct until ventral to the p3-p4, whereas it is much less distinct in *B. cuillinensis*.

Etymology: Species name from noun serendipity, defined as the faculty of making happy and unexpected discoveries by accident.

Holotype

Partial left dentary, BRSUG 20570.

Description

The holotype BRSUG 20570 is a partial left dentary, removed from matrix, with nine teeth in their alveoli (one only comprising roots). It measures 11 mm in length.

Stratigraphic provenance

Kilmaluag Formation, Late Bathonian, Middle Jurassic (*Retrocostatum* Zone: Barron *et al.*, 2012)

Type locality

Just south of Cladach a' Ghlinne, Strathaird Peninsula, Isle of Skye, Scotland UK (Fig. 1).

Referred material

From the Kilmaluag Formation, Isle of Skye: NMS G.1992.47.121.1, partial skeleton.

***BOREALESTES CUILLENSIS* SP. NOV.**

Zoobank registration: LSID urn:lsid:zoobank.org:act:E2EDCA4C-B0F7-46F1-AB7A-118C3575BE69

Differential diagnosis

Borealestes cuillinensis resembles *Borealestes serendipitus* in most features of upper molars, but differs in having a more rounded cusp A, so that there is no anterior crest and no anterolabial crest on cusp A (Figs 5 and 6). *B. cuillinensis* has a shorter anterolingual crest on cusp X than *B. serendipitus*, with a cuspule on the crest. Cusp Z is reduced compared to *B. serendipitus*. The anterior fovea is less distinct than in *B. serendipitus*. In the lower dentition, *B. cuillinensis* is almost indistinguishable from that of *B. serendipitus*, except for having slightly more pointed molar cusps. The lappets of the dentary do not enclose the cartilage of the Meckel's sulcus of *B. cuillinensis,* unlike in *B. serendipitus*, and the mandibular symphysis is less distinct in *B. cuillinensis* than in *B. serendipitus* (Fig. 7).

Etymology

Species named for the Cuillin, a mountain range on the Isle of Skye, Scotland, which overlooks the holotype locality; the skyline of the mountain range resembles the cusps and ridges of the teeth.

Holotype

NMS G.2020.4.1.1, a partial skull and postcranial remains (Fig. 3).

Description

The holotype NMS G.2020.4.1.1 is a partial skeleton that, following preparation for high-resolution CT scanning, is contained within a series of small blocks of blue-grey micritic limestone between ~2-5 cm length. The dentaries and some skull elements are partially visible on the surface, and within the rocks are the skull, vertebrae, scapulacoracoid, humerus, radii, ribs and pes and manus elements. We infer that NMS G.2020.4.1.1 is an adult individual, as the

last (ultimate) lower molar is positioned directly in front the coronoid process, as in adult specimens of *Docodon victor* (Schultz *et al., 2*017).

Stratigraphic provenance

Kilmaluag Formation, Late Bathonian, Middle Jurassic (*Retrocostatum* Zone: Barron *et al*., 2012).

Type locality

Cladach a' Ghlinne, Strathaird Peninsula, Isle of Skye, Scotland UK (Fig. 1).

Referred material

From the Kilmaluag Formation, Isle of Skye: Partial left dentary BRSUG 20571; NMS G.2018.27.1, fragment of right dentary in matrix. From the Forest Marble Formation of Kirtlington, Oxfordshire: NHMUK PV M46394, NHMUK PV M46448, NHMUK PV M46580, and NHMUK PV M46871, all upper molars. NHMUK PV M46316, NHMUK PV M46396, and possibly NHMUK PV M46607 (uncertain), all upper molars.

***Dobunnodon* gen. nov.**

Zoobank registration: LSID urn:lsid:zoobank.org:act:46E0C61F-64A3-4B30-8780-AB634A882043

Type species: 'Borealestes' mussettae Sigogneau Russell, 2003

***Dobunnodon mussettae* (Sigogneau-Russell, 2003) comb. nov.**

Borealestes mussetti Sigogneau-Russell, 2003

Borealestes mussettae Averianov, 2004 (emended gender).

Differential diagnosis

Dobunnodon mussettae resembles other docodontans in that it possesses an anterior 'pseudotalonid basin' on the lower molars, formed by cusps a, b, and g, has cusps b–a–c in a triangular arrangement, the lower molars are elongated anteroposteriorly, with labial row of higher cusps arranged in anteroposterior alignment with largest cusp a, and it has a lingual row of smaller cusps with distinctive anterior cusp g and larger posterior cusp c. The lower molar of *Dobunnodon* is unlike most docodontans, but is similar to *Tashkumyrodon*, in being mediolaterally compressed. It resembles most docodontans, but differs from *Borealestes,* in that the a–g crest is present on both cusp g and cusp a, and in having a strong a–d crest on cusp a (Fig. 5). Cusp g is slightly more developed, and cusps c and g are placed further apart anteroposteriorly, than in *Borealestes*. Unlike *Simpsonodon*, *Agilodocodon*, and *Docodon*, but like most other docodontans*, Dobunnodon* lacks creases and pits, 'ornamentation' on the teeth. *Dobunnodon* has an anterior lingual cingulid that passes below cusp g to midway along the molar anteroposteriorly. The df cusp is more developed in *Dobunnodon* than in *Borealestes* and is distinct from the d cusp. Cusp e is positioned in alignment with the anteroposterior axis of the molar, whereas cusp e is lingual of the anteroposterior axis on molars of *Borealestes*. The upper molars are not yet known for this taxon.

Etymology: The genus name was given for one of the Iron Age Celtic tribes, the Dobunni, that occupied the region around Kirtlington where the holotype was discovered. The species name was given in honour of Dr Frances Mussett for her 'major participation in the accumulation of the Kirtlington fauna' (Sigogneau-Russell, 2003).

Holotype

NHMUK PV M46495, a right lower molar (Fig. 5C)

Description

The holotype NHMUK PV M46495, is a single right lower molar, lacking a root, and broken at the base of cusp a (reconstructed for Fig. 5C), previously described by Sigogneau-Russell (2003) and Panciroli *et al.* (2019).

Stratigraphic provenance

Forest Marble Formation, Late Bathonian, Middle Jurassic (*Retrocostatum* Zone: Barron *et al.,* 2012).

Type locality

Kirtlington Cement Quarry, Oxfordshire, UK.

Referred material

From the Forest Marble Formation of Kirtlington, Oxfordshire: NHMUK PV M46224, NHMUK PV M46239, NHMUK PV M46001, NHMUK PV M46066, NHMUK PV M46836, NHMUK PV M46319, NHMUK PV M46809, and NHMUK PV M46835, all lower molars. From the Forest Marble Formation of Watton Cliff, Dorset: NHMUK PV M46001, lower molar.

DENTAL AND MANDIBULAR MORPHOLOGY

The fossil record for Mesozoic mammaliaforms comprises a disproportionate amount of individual teeth and dentary fragments. It is common practice to use this sparse material as the basis for erecting new species and taxonomic groups, thanks to the complexity of mammaliaform teeth making them a reliable basis for systematic diagnoses. However, it has been recognised that this practice may result in 'over-splitting' (erecting new groups based on

over-interpretation of small differences in molar morphology). For example, the near complete tooth row of *Palaeoxonodon* recovered recently on Skye was found to encompass the diagnostic characters identified as the basis for previously erecting three different species in two genera (Close *et al*., 2016). On the other hand, a lack of variation at certain loci on the lower tooth row between species can result in failing to recognise taxonomically distinct morphospecies, as shown here.

The lack of distinguishing features between the molars in the two *Borealestes* species, *B. serendipitus* and *B. cuillinensis,* means that these two taxa cannot be identified from individual lower molars alone. Nevertheless, we present features of upper molars (Fig. 5A and B) and dentary (Fig. 7, see below) that we consider distinct and indicative of the presence of distinct morphospecies. Many isolated lower molars and dentary fragments previously assigned to *B. serendipitus* (e.g. Sigogneau-Russell, 2003; Panciroli *et al*., 2019) therefore lack diagnostic features at the level of species and must be considered as *Borealestes*. sp. This observation has implications for our understanding of the taxonomic diversity of docodontans, and Mesozoic mammals more generally, suggesting the potential for 'hidden' species that are not recognisable from isolated lower molars.

The holotype of *Dobunnodon mussettae* (='*Borealestes' mussettae* in previous taxonomic designation) is a lower molar, and the upper molars previously assigned to '*Borealestes' mussettae* (Sigogneau-Russell 2003: fig. 4 and Panciroli *et al.,* 2019) match the morphology of the uppers of NMS G.2020.4.1.1, which are found in unequivocal association with the lower molars and partial skeleton. We propose here that these upper molars (NHMUK PV M404, PV M46394, NHMUK PV M46448, NHMUK PV M46580, and NHMUK PV M46871) should be therefore reassigned to the new taxon, *B. cuillinensis*. The features of the lower molars of NMS G.2020.4.1.1 - the a-g crest being absent, and a poorly developed df cusp – are diagnostic for *Borealestes* and distinguish it from *Dobunnodon*.

Only the first lower molar of *Borealestes* share two features with those of the holotype of *Dobunnodon*: a low width-to-length ratio, and wider gap between cusps c and g (Table 2). Nevertheless, this is not present in the rest of the tooth row in *Borealestes.* Low width-to-length ratio, and wider gap between cusps c and g are also seen in other docodontans in which the m1 is known, which suggests that these may be problematic features upon which to erect new docodontan taxa.

DESCRIPTION

Morphology of Borealestes serendipitus *and* Borealestes cuillinensis

NMS G.1992.47.121.1 comprises a partial skeleton of *Borealestes serendipitus* on a block of blue-grey limestone. The block measures approximately 183 mm in length, 105 mm in width, and between 148 mm and 340 mm in thickness. The surface of NMS G.1992.47.121.1 is undulating, with several hairline cracks visible in the prepared upper surface, also visible in synchrotron CT data. Skeletal elements are scattered on the surface of the block, including the palate and elements of the skull (Figs 2 and 8). Synchrotron CT data revealed vertebrae, ribs, radius, partial humerus, ilium, femur and manus and pes elements within the block (unpubl. data EP). The surface bones sit on 'platforms' of rock, the result of acid and mechanical preparation, whereby the surrounding rock was removed. At least seven such platforms no longer contain fossil material, and likely indicate the original positions of bones that have been removed or detached during handling, such as the petrosal NMS G.1992.47.121.2 (Panciroli *et al*., 2018a) and the dentary (NMS G.1992.47.121.3 (Panciroli *et al*., 2019).

NMS G.2020.4.1.1 comprises a partial skeleton of *Borealestes cuillinensis* contained within a series of small blocks of blue-grey limestone between ~2-5 cm length (Fig. 3). The skull is present between two of these blocks, which were broken apart across a natural crack in the limestone. The left dentary is visible on the surface along with the right squamosal and part of

the occipital condyles. The rest of the skull is contained within the rock and visible through X-ray μCT (Figs 3 and 9).

Skull

Dentary

The right dentary *Borealestes serendipitus,* NMS G.1992.47.121.3 (Fig. 7, Table 3), is nearly complete and was detached from NMS G.1992.47.121.1 during preparation. The posteriormost portion of the left dentary remains on the surface of NMS G.1992.47.121.1 (Figs 2 and 7). The incisors are missing from NMS G.1992.47.121.3, but a single incisor and ventral tip of an incisor root are present in NMS G.1992.47.121.1, located in the matrix underneath the nasals. The damaged remnants of a premolar or molar are located within the matrix near a posterior portion of the left dentary. The tip of the main cusp of this tooth is missing and it is damaged lingually and buccally. The remains of the posterior root are present, but fragmented. It is not possible to give a more exact identification due to the poor preservation.

The left dentary of *Borealestes cuillinensis*, NMS G.2020.4.1.1 is preserved on the surface of the limestone block (Fig. 3, Table 3). It comprises p4 to m5 within an incomplete dentary. The m5 can be reliably identified as the ultimate molar because it has a reduced size and two roots appressed to each other (Fig 6D and 9), which are typical of the most posterior lower molar of a molar series in docodontans (Schultz *et al*., 2017; Panciroli *et al*., 2019). The ultimate lower molar is in alignment with and anterior to the coronoid process on the dentary (Fig. 10A). The dentary has a preserved dentary condyle, most of the coronoid process, and a medial ridge with its protuberance and posterior notch (Fig. 10A and C). The tip of the angular process is preserved, but was broken from the dentary during preparation for scanning. A small section was lost, but the position of the remaining fragment was preserved in the limestone surface, and has been repositioned digitally (Fig. 10B and C). An anterior portion of the right

dentary is present in NMS G.2020.4.1.1, including the tooth row from the canine to m2 (Fig. 11A). An isolated incisor and isolated premolar are also present, separated from the tooth row (Fig. 3B).

The morphology of the lower teeth of both species of *Borealestes* conforms to that previously described for *B. serendipitus* in Panciroli *et al*. (2019). The incisors have a large buccal bulge and slightly recurved cusp. A ridge runs from the tip of the cusp to the base of the crown, where there is a small cuspule along the rim of the base of the crown. The single root is wide, tapering ventrally. The alveoli on the preserved right dentary of *B. serendipitus* indicate that the anterior incisors were strongly procumbent, especially i1. This is also seen in other docodontans such as *Agilodocodon* (Meng *et al*., 2015). The slightly extended lingual cingulum in the m4 of NMS G.2020.4.1.1 is not considered diagnostic. This feature appears more distinct in the m4 of the holotype of *B. serendipitus*, BRSUG 20570 than it is in NMS G.1992.47.121.3, and the lingual cingulum of the m5 in NMS G.1992.47.121.3 appears extended compared to either BRSUG 20570 or NMS G.1992.47.121.3. This suggests it is not a reliable diagnostic feature, but is variable among *Borealestes* species.

The dentary appears slightly more curved dorsoventrally in *B. cuillinensis* than in *B. serendipitus*, particularly the anterior portion of the dentary (Fig. 7). The position of the posteriormost foramen is ventral to p1 in both species (Fig. 11A1, Panciroli *et al.,* 2019). In *B. cuillinensis* the mandibular symphysis is indistinct posterior to the canine (Figs 7B and 10A2). The coronoid process is almost complete in *B. cuillinensis*, and appears tall, with the anterior edge steeply ascending from posterior to the m5 (Fig. 10). The posterior edge of the coronoid process dorsal to the dentary condyle appears to curve posteriorly, but the dorsal-most portion is missing.

Premaxilla

The left and right premaxillae of *Borealestes serendipitus* NMS G.1992.47.121.4, are nearly complete, but have been dislodged from the main block surface and are slightly crushed. The left premaxilla is displaced anteriorly in relation to the right premaxilla. The left premaxilla is also more complete, and holds alveoli for I2 and I3 (Fig. 12A). Identification of incisors is possible due to the presence of the intranarial process on the right premaxilla (Fig. 12A3, A4, and A6), and the position of the anterior premaxillary foramen in relation to I1 and I2 (Fig. 12A6). Incisors I3 and I4 are intact and approximately in life-position, and the root of I2 is in place, but its crown is broken off at the alveolar margin and missing. In the right premaxilla, the alveoli for I1-3 are present, although the lateral margin of the premaxilla is more fragmented. The I3 alveolus is crushed, and I3 is not present, but I1-2 are both present and approximately in position, with some displacement. Only a fragment of the right premaxilla is preserved in *Borealestes cuillinensis* NMS G.2020.4.1.1 (Fig. 11B). This fragment is incomplete medially, but contains the alveoli with the I2 and I3 in situ and undamaged, and the I1 is sitting next to the I1 alveolus.

In both species of *Borealestes* the incisor morphology is approximately the same. The upper incisors are slightly recurved with a single-rooted I1 and double-rooted I2-I3. Little of the premaxillary morphology remains in NMS G.2020.4.1.1, but based on this fragment and the preserved maxilla (below), the premaxilla contains only I1-I3, and is shallow dorsoventrally. The I2 and I3 are less caniniform than in *B. serendipitus* NMS G.1992.47.121.4, and proportionally smaller dorsoventrally. For more detailed description of upper incisor morphology in *B. serendipitus* see Panciroli *et al.* (2019).

The margins of the incisive foramen are intact in *B. serendipitus* NMS G.1992.47.121.1. The anterior edges of the foramen lie mediolaterally parallel to the posterior margin of the I2 alveoli. There is a small projection of the premaxilla, jutting posteriorly into the incisive foramen where the premaxillae contact each other anteriorly, creating a heart-shaped anterior margin to

the foramen Fig. 12A6). Anterior to the incisive foramen are the ventral premaxillary foramen, adjacent to I2. There are also two much smaller foramina medial to the I3 alveoli (Fig. 12A5).

On the ventral palatal plate of the premaxillae there are depressions between the alveoli and medial to the toothrow, which are for the receipt of the lower incisor tips when the mouth is closed (Fig. 12A5). The posterior margin of the premaxillae which contacts with the maxilla is not preserved. The anteriormost tips of the premaxillae are preserved, although in poor condition. There is a stump or base of the internarial process on the right premaxilla—this makes identification of the right I1 certain. In the interior of the premaxilla there is a canal connecting from the anterior premaxillary foramen to the ventral premaxillary foramen (Fig. 12A6). The anterior opening of this canal is exposed on the broken anterior surface of the left premaxilla (Fig. 12A4). Posteriorly this canal is traced to the ventral premaxillary foramen, to which the canal is connected from inside the premaxilla. This canal splits into branches in the interior of the right premaxilla. These canals cannot be traced as extensively in the right premaxilla due to poor preservation, but part of this incomplete canal is present in the right premaxilla, and connects the ventral premaxillary foramen laterally toward the interdental gap between I1 and I2.

The lateral surfaces of the premaxillae are more or less vertical from the alveolar margins. The dorso-ventral depth of the premaxilla increases posteriorly, from ~0.5 mm anterior to I2, to ~2.4 mm at the alveolus of I3, and the alveolus of I4 is in the anteriormost portion of the maxilla (see below). The posterior margin of the I4 alveolus is missing. On the endocranial surface of the premaxillae, a groove runs from the endocranial openings of each of the ventral premaxillary foramen, meeting in the midline across the sutures. This creates a canal between the endocranial openings of the ventral premaxillary foramen.

Maxilla and palatine

In *Borealestes serendipitus* NMS G.1992.47.121.1 the maxillae are complete from P4/P5 posteriorly to the broken maxillary base of the zygomatic arch (Figs 13 and 14, Table 3). Teeth are preserved from P4-M4, but are damaged. The facial part of the anterior maxilla is not complete, and the premolar-bearing margin of the maxilla is missing, so the exact count of the premolars is not known. But five upper premolars can be reconstructed based on the lower premolar number on the complete mandible of the specimen (right dentary, NMS G.1992.47.121.3, Fig. 7). The palatal processes of both maxillae are fragmented; the right maxilla is more complete. Both maxillae have preserved the cheek teeth in life-position—the right P4 to M4, and left P5 to M4. The crowns of these teeth, especially the premolars, have been abraded. This ventral surface of the palatal plate of the maxillae, which contain the teeth, was uppermost on the matrix when the fossil was found (Fig. 2). The worn surfaces of the teeth are not due to dental occlusion, but due to taphonomic abrasion. Upper premolar and molar morphology for *B. serendipitus* NMS G.1992.47.121.1 was presented in Panciroli *et al.* (2019).

The left maxilla of *Borealestes cuillinensis* NMS G.2020.4.1.1 is almost complete, with only the section between P1 and P4 mostly missing, except for a fragment of the lateral surface dorsal to the position of P1-P3 (Fig. 15, Table 3). Teeth are well preserved from I4-P1, and P4-M4. The I4 alveolus is enclosed by the maxilla (Fig. 15A1-2), unlike in *B. serendipitus*, in which the I4 alveolus is enclosed by the premaxilla (Fig. 12A). The I4 (which is displaced but complete in NMS G.2020.4.1.1, Fig. 15A1-2) is not caniniform, unlike in *B. serendipitus*. There is a depression for the lower canine tooth tip to rest in when the mouth is closed, positioned between the I4 and C (Fig. 15A2). The P1 is small, but has a recurved main cusp and small posterior cuspule. A distinct diastema separates the P1 from the P2 alveolus in NMS G.2020.4.1.1 (Fig. 15A1-2). The P2 is not present and the anterior of the maxilla is dorsoventrally tall, bulging laterally at the level of the canine, and constricting medially at the diastema (Fig. 15A2-3). There is a foramen dorsal to the space between the I4 and canine

alveoli. A larger infraorbital foramen is dorsal to the P5, and there is a possible foramen dorsal to M1.

Although the right maxilla of *B. cuillinensis* NMS G.2020.4.1.1 is damaged, it includes the tooth row from P3-M4 and a large portion of the maxilla itself, although broken into three pieces (Fig. 16A). The P3 to M1 are damaged. In the left and right maxilla the maxillary base of the zygomatic arch is preserved, and it appears in the left maxilla to project posteriorly beyond the maxilla-palatine suture posterior to the ultimate molar. In the left maxilla the palatal process is present, but displaced ventrally (Fig. 15A2). The medial edge of the palatal process of the maxilla is dorsoventrally deep. As in *B. serendipitus,* the posterior part of the maxilla holds the ultimate molar and its roots. The contact between the maxilla and palatal process of the palatine appears to have been close to the lingual edge of the molar row as in *B. serendipitus*, but the maxilla is broken here and so this interpretation is uncertain. We interpret a separate bone fragment preserved in NMS G.2020.4.1.1 as the palatal process of the right maxilla of *B. cuillinensis* (Fig. 16B). It includes the posterior rim of the process (which is missing the more complete left maxilla), and indicates that it projected posteriorly into the palatal process of the palatine.

The palatal process of the maxilla in *B. serendipitus* NMS G.1992.47.121.1 continues posteriorly until approximately the level of the M2/3 (Fig. 13A1). Crushing and displacement of the medial portion of the palatal process of the maxillae makes this area difficult to interpret. The greater palatine foramen is preserved medial to M2, and the palatal process of the maxillary bone appears to project posteriorly into the palatal process of the palatine bone along the midline suture. This projection has a low ventral anteroposterior ridge. An alternative interpretation is that the palatal process of a maxilla ends at M2/3, and the “projection” aforementioned may be the palatal process of the palatine. The posteriormost portion of the palatal process of the maxillary bone is not preserved in the left maxilla.

The posterior part of the maxilla holds the ultimate molar and its roots. The contact of the maxilla with the palatine appears smooth. The contact between the maxilla and palatal process of the palatine appears to have been close to the lingual edge of the molar row, but as the maxilla is broken here, this interpretation has some uncertainty. A fragment of the right palatine indicates that the suture may have been as little as 0.4 mm from the lingual margin of the alveolus of the ultimate molar. The maxillary base of the zygomatic arch is better preserved in the right maxilla, and does not appear to posteriorly project beyond the maxilla-palatine suture posterior to the ultimate molar (Fig. 13).

The suture of the maxilla-lacrimal slopes posteroventrally from a point dorsal to M2, to P4, overlapping the ventralmost portion of the lacrimal (Fig. 13A2 and 14B). Although the lateral wall of the maxilla is somewhat compressed (a post-mortem distortion) it is clearly laterally convex. The lateral portion of the left maxilla is not preserved.

The lateral surface of the maxilla shows three anterior foramina of the infraorbital canal. These foramina are dorsal to the roots of the P5/M1 junction, P4/P5 junction, and P3/P4 junction of the right maxilla (Fig. 13A).

Crushing makes it impossible to reconstruct most of the endocranial surface and internal structure of the maxilla (Fig. 14A). However the groove on the posterior endocranial surface of the maxilla for the lacrimal is well preserved on both maxillae. Compression has also distorted the shape of the palatal surface of the maxilla, tilting the tooth row mediodorsally.

Nasals

Three fragments of the nasal bone are preserved in *Borealestes serendipitus*: the right and left from just anterior to the anteriormost projection of the lacrimal, to just anterior to the suture with the frontal (the latter suture line is not preserved) (Figs 13 and 14). There is also an anterior fragment of the left nasal (Fig. 12B). The anterior fragment of the left nasal is separated from the rest of the skeleton and is attached to the premaxillae by a small portion of matrix and

Paraloid, as part of NMS G.1992.47.121.4. It includes an anterior foramen on the exterior dorsal surface (Fig. 12B3-4). There is a dorsoventrally deep midline suture where it would have met the right anterior frontal (Fig. 12B2). The nasal in *Borealestes cuillinensis* NMS G.2020.4.1.1 is badly broken, but preserves what appears to be the edge of the anterior nasal foramen, which appears to be large, and the ridge of the nasal-maxilla suture along its length (Fig. 17A3).

The rim of the anterior nasal notch in *B. serendipitus* indicates the notch was wide and terminated 1.6 mm anterior to the anterior nasal foramen. The nasal is narrow anteriorly, widening and extending under the maxilla posterolaterally. A ridge is present on the lateral side of the nasal, where it sat under the anterior edge of the maxilla (Fig. 12B3-4), and presumably under the septomaxilla, although neither those bones nor their facets are preserved.

On the endocranial surface of the nasals of *B. serendipitus*, strong ridges run anteroposteriorly along the length of this section of the nasal (Fig. 12B). These ridges are not visible in the larger posterior portions of nasal. the portion of the right nasal is preserved in *B. cuillinensis* NMS G.2020.4.1.1, is identified by similar endocranial ridges running anteroposteriorly along the endocranial surface (Fig. 17A1). We tentatively interpret these ridges as the remnants, or incompletely preserved base of, the naso-turbinates (Fig. 12B1-B2). They are not well enough preserved in either *Borealestes* specimen to further interpret their structure.

In *B. serendipitus* posterior nasal portions are much wider than the anterior portion, and their midline suture is dorsoventrally deep and forms a projecting ridge endocranially where they join (Fig. 14A-B). Crushing has distorted the original shape of the nasals, making them appear flatter than they may have been in life. The posteriormost nasal foramen is positioned mediolaterally halfway across each nasal on the anterior portion of the preserved bone (Fig. 14B). These foramina open directly into the nasal cavity. Crushing has made it difficult for us to identify or fully reconstruct endocranial structures of the nasals, but nevertheless the broken fragments visible in the CT cross sections (Fig. 14A) sitting between the nasals and the maxillae

are likely the crushed and incomplete remnants of the naso-turbinates, the incomplete parts of which are also preserved on the underside of the nasal as mentioned above. We tentatively interpret that remnants of the maxillary turbinates are preserved on the inner surface of the maxillary, but the maxillary turbinates themselves are not well preserved enough to be reconstructed.

Lacrimals

Both lacrimals are preserved in *Borealestes serendipitus* NMS G.1992.47.121.1: the right lacrimal is in natural articulation with the maxilla (Figs 13 and 14), and the left lacrimal is located on the surface of the block, posterior to the maxillae (Fig. 14C). The right lacrimal is more complete than the left. Only the right lacrimal is preserved in *Borealestes cuillinensis* NMS G.2020.4.1.1, including the zygomatic process of the lacrimal, and the lacrimal foramen (Fig. 18). The orbital flange is broken and not present in this specimen.

The morphology of the lacrimal is similar in both species of *Borealestes,* but the lacrimal is less convex laterally in *B. cuillinensis* than in *B. serendipitus.* The zygomatic process of the lacrimal is long and slender and extends to the line of the posterior edge of the ultimate molar in *B. serendipitus*, and sits in a dorsal groove of the maxilla, where they form the anterior base of the zygomatic arch (Figs 13A2, 14B and 18). It has a distinct lateral groove to receive the jugal. In *B. serendipitus* the orbital flange of the lacrimal extends posteriorly at least as far as the end of the zygomatic process, but in neither specimen of *Borealestes* is the suture with the frontal preserved.

The dorsal and ventral lacrimal foramina are large (Figs 13A2 and B, 14B-C and 18). The lacrimal is laterally convex, and endocranially the surface is domed, with two dorsoventral ridges: one on the orbital flange of the lacrimal, posterior to the lacrimal foramen; the second anteriorly, on the facial extension of the lacrimal (Figs 13B3, 14C4 and 18A2). On the lateral exterior surface of the lacrimal, the ridge that receives the jugal posteriorly runs along the length

of the lacrimal anteriorly, where it marks the edge of the maxilla (Figs 13A2 and B4, 14C2 and 18A1). Ventral to this groove, the lacrimal sits underneath the lateral surface of the maxilla (Figs 13A2 and 14B and C2). The anteriormost portion of the facial extension of the lacrimal is not preserved on either species of *Borealestes*, and it is unclear how far it extends, or how it meets the nasal and maxilla anteriorly.

Frontals

A fragment of the dorsomedial portion of the left frontal of *Borealestes serendipitus* is located beside the postparietal on the surface of the block of limestone NMS G.1992.47.121.1 (Fig. 2). The interfrontal suture is partly preserved (Fig. 19A). Although somewhat damaged along its edge, it is clearly vascularised internally (Fig. 19A1), and thickens anteriorly. This thickening is due to a transverse ridge on the endocranial surface, which we interpret as the ridge on the frontal that corresponds to the circular or annular fissure separating the posterior margin of the fossa for the olfactory bulb from the anterior margin of the fossa for the cerebral hemisphere, if the brain endocast were intact and fully preserved (Fig. 19A2). A similar ridge is seen on the brain endocast of the mammaliaform *Morganucodon* (Kermack *et al*. 1981; Rowe *et al*. 2011) and later mammaliaforms.

The posterior of the frontal bone, where it meets the interparietal, is not preserved, nor is the lateral wall. The remnants of an anteroposterior indentation and ridge on the external surface of the frontal, sloping posteroventrally, is interpreted as either an orbital ridge, or as marking the extent of the anterior overlap of the parietal bone (see below) (Fig. 19A3 and A5). As the anteriormost portion of the parietal is not preserved, it is not possible to confirm this.

Anteriorly, a possible foramen could correspond to the infraorbital foramen of *Haldanodon* (Lillegraven & Krusat, 1991) (Fig. 19A3). However, this area is damaged and the anterior portion missing so this identification is not certain.

Parietals

The left parietal is the largest preserved portion of the cranium of *Borealestes serendipitus* NMS G.1992.47.121.1, with most of it present including the medial interparietal suture, the parietal-postparietal suture, and multiple lateral fragments (Fig. 20). The posterior of the cranium formed by the parietal is transversely wide, with a small sagittal crest at the dorsoventrally deep suture between the left and right parietals. Where the interparietal suture meets the postparietal suture, the parietal contributes to a dorsal projection of the sagittal crest. The parietal is overlapped by the postparietal along the posterior margin, forming a slight nuchal crest running posterolaterally (Fig. 20B and D).

The walls of the parietal are thin, except along the interparietal suture where the parietals are thicker and contribute to the sagittal crest. The lateral part of the parietal in the temporal area is also thickened. This corresponds to a bulge on the endocranial surface, which we interpret as marking the rim of the indentation of the meninges of the left side of the cerebellum and left cerebral hemisphere. This ridge is concurrent with the low ridge associated with the transverse sinus sulcus, as seen on the endocranial surface of the parietal in the skull roof of *Morganucodon* (Kermack *et al.* 1981: fig 31) (Fig. 20A and C). On the exterior posterolateral wall of the parietal, a ridge running parallel to the nuchal crest probably marks the overlapped edge of the dorsal flange of the squamosal (Fig. 20B and D).

The identity of an indentation on the anterior dorsolateral surface of the parietal (Fig. 20B) is uncertain. Crushing and flattening of the bone here makes interpretation difficult and hinders reconstruction, but there are three possibilities: 1) it represents post depositional damage; 2) it marks the posterodorsal overlap of the bones of the temporal region; or 3) it resulted from the bite of a predator or scavenger. We consider the third possibility to be the least likely, and favour the second interpretation, which would suggest that the bone located anteroventrally below this indentation could be a fragment of the temporal region.

Postparietal

The postparietal of *Borealestes serendipitus* is approximately triangular in shape along the dorsal edge where it meets the parietals (Fig. 19D). It slopes posteroventrally towards the supraoccipital (not preserved). The posteroventral edge of the postparietal is not preserved. A small projection of the postparietal inserts between the parietals posterior to the interparietal suture, and this forms the dorsalmost projection of the sagittal crest. Laterally in both directions, the postparietal overlaps the posterior edge of the parietals, contributing to a nuchal crest.

There is a gentle bulge along the midline of the postparietal, forming a midline ridge (Fig. 19D1). There are a series of foramina along the exterior dorsal side of the postparietal. The postparietal is well vascularised, including along the length of the medial ridge (Fig. 19D3). The endocranial surface of the postparietal is unclear—the limited contrast in the synchrotron CT data between this section of the fragment and the matrix it sits upon make digital segmentation problematic. However, there is an endocranial swelling that mirrors the exterior medial ridge of the postparietal. Posteroventrally the postparietal thins, but the suture with the posteriormost portion of the cranium is missing.

Petrosals

The petrosals of *B. serendipitus,* NMS G.1992.47.121.1 and NMS G.1992.47.121.2, have previously been described (Panciroli *et al.*, 2018a). Both petrosals are preserved: the right petrosal is more complete, and still attached to the matrix as part of NMS G.1992.47.121.1. The left petrosal NMS G.1992.47.121.2 is less complete, and is separate from the rest of the skeleton.

Squamosal

The right squamosal of *Borealestes serendipitus* is preserved in NMS G.1992.47.121.1, located beside the occipital condyles, separated from the rest of the skull, and below the surface

of the block (Figs 2 and 19B). The right squamosal of *Borealestes cuillinensis* is well preserved in NMS G.2020.4.1.1 (Fig. 21A), along with the anterior tip of the zygomatic process of the left squamosal (Fig. 21B).

The squamosal of *B. serendipitus* shows a long and slender zygomatic process (Fig.19) . In *B. cuillinensis* the zygomatic process narrows anteriorly and has a distinct ridge along its length on the dorsal margin (Fig. 21A2), giving it a comparatively more robust appearance, more similar to the squamosal glenoid and zygoma of *Haldanodon* (Lillegraven & Krusat, 1991; Ruf *et al*., 2013).

In both *Borealestes* species there is a wide glenoid fossa for articulation with the dentary condyle, although it is slightly wider in *B. cuillinensis* (Fig. 21A1 and A3). In both species the squamosal glenoid is a shallow and concave structure with a slightly raised postglenoid ridge, and the glenoid appears to have an oval outline in ventral view narrowing anteriorly in a teardrop shape (Figs 19B and 21A). The beginning of a distinct postglenoid ridge is preserved in *B. cuillinensis* NMS G.2020.4.1.1, but part of it is missing laterally. The more complete squamosal of this specimen suggests the squamosal projected less laterally than in *B. serendipitus*, but that the skull would have a similar elongate triangular shape (Figs 8 and 9).

As for all docodontans there is a constriction in the neck of the glenoid in both species of *Borealestes,* visible medial to the glenoid (Fig. 19A2 A3, and 21A), for example as seen in *Haldanodon* (Luo 1994; Ruf *et al*. 2013). Although the lateral extent of the constriction cannot be determined in *B. serendipitus* NMS G.1992.47.121.1 because this lateral margin of the glenoid is damaged, the constriction appears to be less pronounced in *Borealestes* species than *Haldanodon*.

There is a large, broadly concave surface on the medial aspect of the squamosal cranial moiety in *B. serendipitus* NMS G.1992.47.121.1, which we tentatively identify as the contact of the squamosal to the lateral side of the paroccipital process of the petrosal, but this area is not well preserved. The part of the squamosal that would contact the paroccipital process of the

petrosal extends from just posterior to the glenoid fossa medially to a depression called the entoglenoid recess (sensu Ruf *et al*., 2013: fig. 2—this is the same as the ventromedial squamosal recess of Lillegraven & Krusat, 1991). The right petrosal of *B. serendipitus* is preserved but is separated from the squamosal (see Panciroli *et al.* 2018). Unfortunately the junction between the right petrosal and the right squamosal is not preserved well enough to interpret the other features expected to be located in this area, such as the crista parotica and the fossa incudis, both of which are missing.

In *B. cuillinensis* part of the cranial moiety of the squamosal is preserved, and has a strong dorsal ridge that curves anterodorsally (Fig. 21A2 and A4-5). The entoglenoid recess (= the ventromedial squamosal recess of Lillegraven & Krusat, 1991) and external auditory meatus are preserved (Fig. 21A1 and A3). The entoglenoid recess is shallow concave structures medial to the glenoid fossa, and it bears resemblance that of *B. serendipitus*. However, the crista parotica and the fossa incudis in the adjacent region of the petrosal are not preserved, and it is not feasible to interpret these and other structures in the junction regions of the squamosal and the petrosal.

Occipital condyle and exoccipital

In *Borealestes serendipitus* NMS G.2020.4.1.1 the exoccipital and occipital condyles are separated from the skull, and are preserved within the matrix beside the right squamosal (Fig. 2). The occipital condyles of *Borealestes cuillinensis* NMS G.2020.4.1.1 are located on the surface of the limestone, resting against the left dentary (Fig. 3). Fragments of the exoccipital are attached to the left occipital condyle (Fig. 21C), but they are poorly preserved.

The occipital condyles appear indistinguishable between the species of *Borealestes.* We tentatively identify the odontoid notch in the occipitals. However it is uncertain whether the exoccipitals contacted at the midline dorsomedially, ventral to the postparietal. Due to a lack of preservation, there may have been a slight gap in the contact with the supraoccipital (Figs 19C

and 21C). On the preserved part of exoccipital of *Borealestes serendipitus*, the interior of the bone appears to be hollow and trabeculated. The pars cochlearis of the petrosal shows multiple vascular channels including circumpromontorial plexus through the bone in *B. serendipitus* (Panciroli *et al*., 2018). The paroccipital region of the petrosal exhibits pneumaticity (e.g., paroccipital pneumatic recess) as in *Haldanodon* (Ruf *et al*. 2013), and the pneumatic space in the middle ear appears to be connected to the well developed vascular plexus structure inside the paroccipital region and in the adjacent exoccipital. The trabeculated and hollowed interior spaces of the petrosal and exoccipital would have been filled with vasculature and/or bone marrow (Ruf *et al*. 2013: fig. 4). Even the occipital condyles are hollow and trabeculated (Ruf *et al*., 2013: fig. 3D and 4: 'condylar plexus'). The hollowed interior of the exoccipital, especially the occipital condyle of *Borealestes*, appears to be similar. Based on this, it is interpreted here that the exoccipital bone has similar interior vascularised and trabeculated interior structure in *Borealestes*, as interpreted for docodontans as a whole. The occipital condyles project from the base of the skull and are oval in shape. The jugular process of the right exoccipital is preserved on the ventral side, although there is damage to the ventral aspect of the exoccipitals. The basioccipital is not preserved.

DISCUSSION

Phylogenetic Analysis and Position of Dobunnodon mussettae

The phylogenetic analysis support the erection of a new species of Borealestes, and the placement of '*B*.' *mussettae* into a new genus. The species '*Borealestes' mussettae* was erected based on the holotype lower molar and associated upper molars (Sigogneau-Russell 2003). However, the new material assigned to *B. cuillinensis* (NMS G.2020.4.1.1) herein includes upper molars that match those assigned to '*B.' mussettae* by Sigogneau-Russell (2003) and Panciroli *et al*. (2019), confirming that all upper molar material previously assigned to '*B.' mussettae* belongs instead to *B. cuillinensis.* Therefore, the hypodigm of '*B*.' *mussettae*

now includes only lower molars, which can be compared to the type specimen (see *Systematic Palaeontology*). Previous phylogenetic analysis that recovered '*B.' mussettae* and *B. serendipitus* as sister taxa was based on both the upper and lower molar characters (Panciroli *et al.* 2019). These species were previously united particularly by the character of the presence of an anterior fovea (*sensu* Panciroli *et al.* 2019) at the buccolingual midpoint of the upper molar, a feature that can no longer be said to be present in '*B*.' *mussettae*.

The remaining '*B.' mussettae* lower molars differ significantly from those of *Borealestes*, therefore it is justified to place it in the new genus, *Dobunnodon*. In *Dobunnodon* the a–g crest is present on cusp g and cusp a, and there is a strong a–d crest on cusp a – both of these features are absent in lower molars in *Borealestes* species (Fig. 6). Cusp g is slightly more developed in *Dobunnodon*, and cusps c and g are placed further apart anteroposteriorly than in *Borealestes.* The more developed cusp df - distinct from the d cusp - and the more central position of the cusp e (mediolaterally) all differentiate this taxon from *Borealestes*. Based on these differences and without the upper molar characters that had united these taxa in Panciroli *et al.* (2019), we consider there to be sufficient grounds to separate these taxa at genus level. *B. serendipitus* was named first, so we place '*B.' mussettae* in the newly erected genus, *Dobunnodon*, retaining the original species name (Sigogneau-Russell, 2003).

Crania

Anterior cranial elements

Borealestes serendipitus and *Borealestes cuillinensis* have similar elongate and slender dentary morphology. Nevertheless, specimens available so far suggest they can be interpreted as being distinguished by the morphology of the Meckel's sulcus, which is closed anterior to the position of m3 in *B. serendipitus* but open in *B. cuillinensis*, and the mandibular symphysis, which is more distinct in *B. serendipitus* than in *B. cuillinensis*. However, we accept that with limited material in which the Meckel's sulcus is preserved, this character may be unreliable and

show intraspecific variation. For example, the degree of development of anterior part of the Meckel's sulcus may be age-dependent, as evidenced by growth series of mandibular specimens of *Docodon victor* (Schultz *et al*. 2017). The degree to which the sulcus is open or closed appears to be somewhat variable in specimens of *Morganucodon watsoni* (P. Gill pers. comm.) and variable depending on developmental stage of the mandible in monotremes.

The holotype of *B. cuillinensis* (NMS G.2020.4.1.1) is overall smaller than *B. serendipitus* NMS G. 1992.47.121.1 (and associated material) (Table 2). Size can be unreliable in distinguishing between species, as differences in size may represent differences of growth stage or intraspecific variation. However, patterns of dental eruption suggest that NMS G.2020.4.1.1 is a fully grown adult, in spite of its smaller size. The ultimate lower molar of *B. cuillinensis* (NMS G.2020.4.1.1) is in alignment with and anterior to the coronoid process on the dentary (Fig. 10). In other docodontans with a growth series of younger to older individuals (e.g., *Docodon victor*, Schultz *et al*., 2019), the ultimate molar ends up in front of the coronoid process in the older and fully adult individual as the jaw grows longer.

Most features of the anterior bones of the skulls of *Borealestes* are similar to those seen in other docodontans, but particularly the long, gracile rostrum of *Agilodocodon* (Meng *et al*., 2015). By comparison to the more complete basicranium with intact squamosal and petrosal of *Haldanodon* (Lillegraven & Krusat, 1991), for which there is a more recent reconstruction (Ruf *et al*., 2013), we interpret that the squamosal projects far laterally, making the skull widest at this point and giving the skull an overall triangular outline in the dorsal or the ventral views (Figs 8, 9, 19 and 21).

The anterior lower incisors of *B. serendipitus* are strongly procumbent, especially i1, as seen in *Agilodocodon*. This characteristic was argued in *Agilodocodon* to suggest a possible adaptation for exudativory, with this procumbent morphology resembling that seen in old world monkeys that gnaw on bark to eat sap (Meng *et al*., 2015: 765). This would have been a plausible feeding mode for an arboreal docodontan, but close comparison between extant

exudativores and *Agilodocodon* does not support this idea, as these docodontans do not have features such as restricted labial enamel, broad lower incisor girth, toothcombs and 'short-tusked' canines (Wible & Burrows, 2016). The morphology of the docodontan procumbent incisors more closely resembles extant insectivorous mammals, such as macroscelideans, and this is also supported by the molar morphology.

In the specimen of *B. serendipitus*, NMS G.1992.47.121.4, it is not entirely clear if the premaxilla formed the posterior margin of I4 as in *Haldanodon*, or whether it was formed by the maxilla. In *B. cuillinensis* NMS G.2020.4.1.1, the I4 alveolus is entirely within the maxilla, and the I3 alveolus is formed by the premaxilla. In *Morganucodon* the premaxilla-maxillary suture is located between I3 and I4, with I3 in the premaxilla and I4 in the maxilla (Kermack *et al*., 1981: fig 80), whereas in *Docodon apoxys* this suture runs through the alveolus of I5, and the I5 is completely within the premaxilla (Rougier *et al*. 2015: fig 6). At the anterior end of the right premaxilla in NMS G.1992.47.121.4 the probable stump of the internarial process, or the median process of the premaxillary bone, can be identified, as in *Haldanodon* (Lillegraven & Krusat, 1991:59). This is a plesiomorphic feature retained in mammaliaforms, seen in all docodontans (e.g., Luo *et al.* 2015b: fig. 1) and so although not preserved in NMS G.2020.4.1.1, it was most likely present.

The vascular canals connecting the anterior premaxillary foramen anteriorly and laterally are likely to be for the greater palatine nerve and artery, and similar vascular channels have been traced in pre-mammalian cynodonts (Benoit *et al*., 2016). Some features observed in other docodontans such as *Haldanodon*, that are not preserved in this specimen of *B. serendipitus* include a bulging canine root in the maxilla, the position of the infraorbital foramen just posterior to the canine, presence and position of the septomaxilla, and the "posterior salient" of the premaxillary bone (Lillegraven & Krusat, 1991: 46). The bulging canine root is present in this specimen of *B. cuillinensis*, and the infraorbital foramen is located poster to the canine dorsal to P5 (and smaller foramina are located anterior to the canine, and dorsal to M1). We have

therefore reconstructed the missing portions of the skull of these species of *Borealestes* based on the morphology of these features as present in *B. cuillinensis*, and as seen in other docodontans, notably *Agilodocodon* (Figs 8 and 9).

The greater palatine foramen marks the edge of the palatal process of the maxilla in NMS G.1992.47.121.1, medial to M2, and the palatal process of the maxillary bone may project posteriorly into the palatal process of the palatine bone along the midline suture in NMS G.1992.47.121.1 but it is unclear due to damage to the specimen (Fig. 13A). In *B. cuillinensis* we interpret one fragment of bone as the palatal process of the maxilla, which has a projection that would intrude posteriorly into the palatal process of the palatine bone. Such a projection is not seen in *Morganucodon* nor *Haldanodon*. The position of the greater palatine foramen in *B. serendipitus* differs from *Haldanodon*. In both taxa it is positioned medial and slightly anterior to M2, and there is no greater palatine groove (unlike in *Morganucodon*). But in *Haldanodon* the foramen is oblong, positioned closer to the midline suture, and on the edge of the palatine process of the maxilla. It is not clear whether the posterior rim of the grater palatine foramen in either species of *Borealestes* is formed by the palatine process of the palatine (as in *Haldanodon*), but the foramen is more rounded in NMS G.1992.47.121.1, and positioned closer to the toothrow (Fig. 13A).

Because the external aspect of the maxilla is dorsoventrally compressed in *B. serendipitus* (NMS G.1992.47.121.1, Figs 13 and 14), the two posterior foramina appear relatively small in comparison to the large infraorbital foramina in the maxilla in *Docodon* (Schultz *et al.,* 2017), *Haldanodon* (Lillegraven & Krusat, 1991) and *Docofossor* (Luo *et al*., 2015b). In *B. cuillinensis* (NMS G.2020.4.1.1) the foramen dorsal to P5 appears similar to the large infraorbital foramina in these taxa (Fig. 15A1). Only the rounded posterior edge of the anteriormost infraorbital foramen is preserved. In both *Borealestes* species these infraorbital foramina are located more anteriorly in relation to the tooth row than in *Docodon*: in *Docodon* two infraorbital foramina are located dorsal to the M1/M2 junction and roots of P4 on the lateral

side of the maxilla (Schultz *et al*., 2017: fig. 9). In *Haldanodon* three foramina are located above the roots of the penultimate and ultimate premolars, and the M1 (T. Martin, pers. com.).

The posteriorly mediolaterally broad nasals in *B. serendipitus* more closely resemble *Haldanodon* in their width (Lillegraven & Krusat, 1991:p46), than the slightly narrower skull of *Agilodocodon* (Meng *et al*., 2015), or the greater extension of the maxillae and lacrimals dorsally as seen in *Morganucodon* (Lillegraven & Krusat, 1991). This accentuates the triangular dorsal profile of the skull of *B. serendipitus*, exaggerated further by the wide zygomatic arches (see below). The posterior nasal foramina in *B. serendipitus* are positioned approximately in line with P4, which is more posteriorly positioned and fully enclosed by the nasal than in *Haldanodon*. As in *Haldanodon*, but unlike *Morganucodon*, the nasals extend posteriorly to lie at least in line with the base of the maxillary base of the zygomatic arch. Anteriorly the nasals of *B. serendipitus* resemble *Haldanodon*, with a long projection of the nasal medial to the anterior nasal foramen.

The lacrimal, and what remains of the frontal, resemble other docodontans and basal mammaliaforms such as *Morganucodon*.

Posterior cranial elements

The small sagittal crest along the unfused medial contact of the parietals of *B. serendipitus* NMS G.1992.47.121.1 is similar to that seen in other docodontans, but is slightly less prominent than in *Haldanodon*, or the geologically older basal mammaliaform *Morganucodon*. The nuchal crest is also similar to other docodontans, notably *Haldanodon*. Both of these features are seen variably in other mammal groups, usually associated with muscular attachment and/or sexual dimorphism. However the interparietal described in *Haldanodon* is positioned posteriorly between the parietals and the dorsal edge of the postparietal (Lillegraven & Krusat, 1991:77). In *B. serendipitus*, the postparietal sits against the parietal directly, and a small dorsal projection slots into the parietal suture to contribute to the small sagittal crest (Figs 8, 19D and 20). The bulge along the midline of the postparietal and the

foramina present on the dorsal lateral surface, indicate high vascularisation of this bone, and conform with the form of the postparietal in *Haldanodon*.

The complete morphology of the petrosals of this specimen of *B. serendipitus* has been described previously (Panciroli *et al*., 2018a). The portion of squamosal preserved in NMS G.1992.47.121.1 includes the auditory meatus and the glenoid fossa, and suggests a gracile squamosal and jugal more like *Agilodocodon* (Meng *et al*., 2015) than the more robust squamosal and jugal of *Haldanodon* (Lillegraven & Krusat, 1991). We interpret the squamosal to project far laterally, as in *Haldanodon*, giving the skull a triangular outline from above (Fig. 8). The squamosal of *B. cuillinensis* appears more robust than *B. serendipitus*, with a broader glenoid fossa and slightly deeper zygomatic process (Figs 9 and 21). It remains more gracile than that seen in *Haldanodon*. Most of the dorsal part of the squamosal cranial moiety is not preserved in either specimen of *Borealestes*, but the indentation on the posterolateral side of the parietal in NMS G.1992.47.121.1 suggests it was present and extended approximately a third of the way up the parietal dorsally (Fig. 20B and D), making it more similar to *Morganucodon* than *Haldanodon*. The squamosal glenoid and zygoma in *Borealestes* are similar to those of *Haldanodon* (Lillegraven & Krusat, 1991; Ruf *et al*., 2013). The posteromedial portion of the squamosal (= the cranial moiety of the squamosal) posterior to the glenoid fossa is broken and displaced in *B. serendipitus* (NMS G.1992.47.121.1). However, on the cranial moiety there is the beginning of a strong dorsal ridge (Fig. 20B2)—possibly this ridge would join dorsally with the strong nuchal crest on the lateral aspect of the parietal (Fig. 20), which is the case in the preserved skull of *Haldanodon* (Lillegraven & Krusat, 1991).

The morphology of the occipital condyles in both *Borealestes* species resembles *Haldanodon* (Lillegraven & Krusat, 1991; Ruf *et al*., 2013), and is little changed from other early mammaliaforms such as *Sinoconodon, Morganucodon* and *Megazostrodon* (Jenkins and Parrington, 1976; Kermack *et al*., 1981; Gow 1986; Crompton and Luo, 1993).

The crushing and flattening of the anterior dorsolateral surface of the parietal bone in NMS G.1992.47.121.1 *B. serendipitus* makes it unclear if the indentation there has resulted from pre- or post-depositional damage, or represents a ridge marking the posterodorsal overlap of the temporal bone. If it was the latter, this would suggest the bone located anteroventral to it was a fragment of the temporal region. However the indentation would suggest a strong finger-like projection of the temporal region, which is unlike that seen in other docodontans.

CONCLUSIONS

The partial skeletons of *Borealestes serendipitus* and *Borealestes cuillinensis* comprise the most complete Mesozoic mammal skeletons reported from the British Isles to date. Their exceptional preservation – partially associated and with minimal compression – makes them globally significant. Being Bathonian in age, *Borealestes* is among the geologically oldest docodontans. It is of similar age to *Castorocauda*, *Agilodocodon* and *Microdocodon* of the Tiaojishan Formation directly dated to be about 165 Ma (Ji *et al*., 2006; Meng *et al*., 2015; Zhou *et al*., 2019), and to *Itatodon*, *Hutegotherium* and *Simpsonodon* from the Berezovsk site of the Middle Jurassic Itat Formation in West Siberia of Russia, which is also Bathonian (Averianov and Lopatin 2005; Averianov *et al*., 2010). These *Borealestes* species are of intermediate robustness compared to other docodontans, but share an elongate and slender dentary morphology more similar to *Agilodocodon*. Despite a consensus that Docodonta are closer to crown-group mammals than *Sinoconodon* and Morganucodonta, their skulls retain many plesiomorphic features seen in *Sinoconodon, Morganucodon* and *Megazostrodon*, such as the retention of postdentary bones, and internarial bar, and the morphology of the lacrimal, frontal, and occipital condyles. Most features of the anterior bones of the skulls of *Borealestes* are similar to those seen in other docodontans, but particularly the long, gracile rostrum of *Agilodocodon*. The structure of the petrosal, and complex cusp arrangement of the teeth, are

among the features that distinguish docodontans from other earlier diverging mammaliaforms clades.

The surprising lack of distinguishing features between the lower molars of *B. serendipitus* and *B. cuillinensis,* means that these two taxa do not appear to be identifiable from individual lower molars alone. These species can be distinguished by their upper molars, and by the morphology of the Meckel's sulcus in the dentary (which is closed anterior to the position of m3 in *B. serendipitus* but open in *B. cuillinensis*) and the mandibular symphysis (which is more distinct in *B. serendipitus* than in in *B. cuillinensis*). This observation suggests potentially 'hidden' species may be present in fossil assemblages that are not easily recognisable from isolated molars, and has implications for our picture of the taxonomic diversity of docodontans and Mesozoic mammals as a whole.

ACKNOWLEDGEMENTS

EP was funded during part of this research by NERC grant number NE/L002558/1, with additional funding from the Palaeontographical Society and the Inverness Field Club. Many thanks to Scottish Natural Heritage and John Muir Trust for granting our permits for fieldwork each year on the Isle of Skye. We are grateful to all of the field work teams who have worked on Skye, including Michael Waldman (who has also provided many insights into the site), Andrzej Wolniewicz and Roger Close, who assisted with collection of specimens described herein. We acknowledge the European Synchrotron Radiation Facility for provision of synchrotron radiation facilities, and we would like to thank Paul Tafforeau for assistance in using beamline ID19. Thank you to Stephen Brusatte for his role as supervisor to EP, and along with Ian Corfe and Florian Fusseis provided assistance in obtaining synchrotron beamtime. We would like to thank Tom Davies and Ian Butler for their time and expertise acquiring CT scans. Tapadh leat to Sìne Ghilleasbuig, Dugald Ross, and Roddy Maclean for advice regarding the use of Scottish Gaelic

and local place names for naming. We thank Gemma Baker for insights into the stratigraphic position of NMS G.2020.4.1.1, based upon her undergraduate research project at the University of Birmingham. Many thanks for the detailed comments from our reviewers, Pamela Gill, Guillermo Rougier, and an anonymous reviewer, which helped improve this manuscript.

REFERENCES

Andrews JE. 1985. The sedimentary facies of a late Bathonian regressive episode: the Kilmaluag and Skudiburgh Formations of the Great Estuarine Group, Inner Hebrides, Scotland. *Journal of the Geological Society of London* 142: 1119–1137.

Anquetin J. 2009. A new stem turtle from the Middle Jurassic of Scotland: new insights into the evolution and palaeoecology of basal turtles. *Proceedings of the Royal Society B* 276: 879–886.

Anquetin J. 2010. The anatomy of the basal turtle *Eileanchelys waldmani* from the Middle Jurassic of the Isle of Skye, Scotland. *Earth and Environmental Science Transactions of the Royal Society of Edinburgh* 101: 67–96.

Averianov AO. 2004. Interpretation of the Early Cretaceous mammal *Peraiocynodon* (Docodonta) and taxonomy of some British Mesozoic docodonts. *Russian Journal of Theriology* 3: 1–4.

Averianov AO, Lopatin AV. 2006. *Itatodon tatarinovi* (Tegotheriidae, Mammalia), a docodont from the Middle Jurassic of Western Siberia and phylogenetic analysis of Docodonta. *Paleontological Journal* 40: 668–677.

Averianov AO, Lopatin AV, Krasnolutskii SA, Ivantson SV. 2010. New docodontans from the Middle Jurassic of Siberia and reanalysis of Docodonta interrelationships. *Proceedings of the Zoological Institute of Russian Academy of Sciences* 314: 121–148.

Averianov AO, Martin T, Lopatin AV, Skutschas P, Schellhorn R, Kolosov P, Vitenko, D. 2018. A high-latitude fauna of mid-Mesozoic mammals from Yakutia, Russia. *PLoS One* 13: e0199983.

Barrett PM. 2006. A sauropod dinosaur tooth from the Middle Jurassic of Skye, Scotland. *Transactions of the Royal Society of Edinburgh: Earth Sciences* 97: 25–29.

Barron AJM, Lott GK, Riding JB. 2012. Stratigraphic Framework for the Middle Jurassic Strata of Great Britain and the Adjoining Continental Shelf: Research Report RR/11/06. British Geological Survey, Keyworth. 177 pp.

Benoit J, Manger PR, Rubidge BS. 2016. Palaeoneurological clues to the evolution of defining mammalian soft tissue traits. *Scientific reports* 6: 25604.

Chen M, Luo Z-X, Wilson GP. 2017. The postcranial skeleton of *Yanoconodon allini* from the Early Cretaceous of Hebei, China, and its implications for locomotor adaptation in eutriconodontan mammals. *Journal of Vertebrate Paleontology* 37: e1315425.

Chen PJ, Hudson JD. 1991. The conchostracan fauna of the Great Estuarine Group, Middle Jurassic, Scotland. *Palaeontology* 34: 515–545.

Close RA, Davis BM, Walsh S, Woloniewicz AS, Friedman M, Benson RBJ. 2016. A lower jaw of *Palaeoxonodon* from the Middle Jurassic of the Isle of Skye, Scotland, sheds new light on the diversity of British stem therians. *Palaeontology* 59: 155–169.

Crompton, AW, Luo Z-X. 1993. Relationships of the Liassic mammals *Sinoconodon*, *Morganucodon*, and *Dinnetherium*. In: Szalay FS, Novacek MJ, and McKenna MC eds. *Mammal Phylogeny: Mesozoic Differentiation, Multituberculates, Monotremes, Early Therians, and Marsupials*. New York: Springer-Verlag, 30–44.

Datta PM. 2005. Earliest mammal with transversely expanded upper molar from the Late Triassic (Carnian) Tiki Formation, South Rewa Gondwana Basin, India. *Journal of Vertebrate Paleontology* 25: 200–207.

Evans SE. 1992. Small reptiles and amphibians from the Forest Marble (Middle Jurassic) of Dorset. *Proceedings of the Dorset Natural History and Archaeological Society* 113: 201–202.

Evans SE, Waldman M. 1996. Small reptiles and amphibians from the Middle Jurassic of Skye Scotland. In: Morales M. ed. *The Continental Jurassic*, *Museum of Northern Arizona Bulletin* 60: 219–226.

Gambaryan PP, Kuznetsov AN, Panyutina AA, Gerasimov SV. 2015. Shoulder girdle and forelimb myology of extant Monotremata. *Russian Journal of Theriology* 14: 1–56.

Gingerich PD. 1973. Molar occlusion and function in the Jurassic mammal *Docodon*. *Journal of Mammalogy* 254: 1008–1013.

Gow CE. 1986. A new skull of *Megazostrodon* (Mammalia: Triconodonta) from the Elliot Formation (Lower Jurassic) of southern Africa. *Palaeontologia Africana* 26: 13–23.

Harper T, Rougier GW. 2019. Petrosal morphology and cochlear function in Mesozoic stem therians. *PLoS ONE* 14: e0209457.

Harris JP, Hudson JD. 1980. Lithostratigraphy of the Great Estuarine Group (Middle Jurassic), Inner Hebrides. *Scottish Journal of Geology* 16: 231–250.

Hu YM, Meng J, Clark JM. 2007. A new Late Jurassic docodont (Mammalia) from northeastern Xinjiang, China. *Vertebrata Palasiatica* 45 :173–194.

Jenkins Jr FA. 1969. Occlusion in *Docodon* (Mammalia, Docodonta). *Postilla* 139: 1–24.

Jenkins Jr FA, Parrington FR. 1976. The postcranial skeletons of the Triassic mammals *Eozostrodon*, *Megazostrodon* and *Erythrotherium*. *Philosophical Transactions of the Royal Society of London B Biological Sciences* 273: 387–431

Ji Q, Luo Z-X, Yuan C-X, Tabrum AR. 2006. A swimming mammaliaform from the Middle Jurassic and ecomorphological diversification of early mammals. *Science* 311: 1123–1127.

Judd JW. 1878. The secondary rocks of Scotland. Third paper. The strata of the western coasts and islands. *Quarterly Journal of the Geological Society of London* 34: 660–743.

Kermack KA, Mussett F, Rigney HW. 1981. The skull of *Morganucodon*. *Zoological Journal of the Linnean Society* 71: 1–158.

Kielan-Jaworowska Z, Cifelli RL, Luo Z-X. 2004. *Mammals from the Age of Dinosaurs: Origins, Evolution, and Structure*. New York: Columbia University Press.

Kretzoi M. 1946. On Docodonta, a new order of Jurassic Mammals. *Anneles Historico-Naturales Musei Nationalis Hungarici* 39: 108–111.

Kühne WG. 1956. The Liassic therapsid *Oligokyphus*. London: British Museum (Natural History).

Lillegraven JA, Krusat G. 1991. Cranio-mandibular anatomy of *Haldanodon exspectatus* (Docodonta; Mammalia) from the Late Jurassic of Portugal and its implications to the evolution of mammalian characters. *Contributions to Geology, University of Wyoming* 28: 39–138.

Luo Z-X. 1994. Sister taxon relationships of mammals and the transformation of the diagnostic mammalian characters. pp. 98–128. In Fraser NC, and Sues H-D, eds. *The Shadow of Dinosaurs: Early Mesozoic Tetrapods.* Cambridge: Cambridge University Press.

Luo Z-X, Kielan-Jaworowska Z, RL Cifelli. 2002. In quest for a phylogeny of Mesozoic mammals. *Acta Palaeontological Polonica* 47: 1–78.

Luo Z-X, Gatesay SM, Jenkins FA, Amaral AA, Shubin NH. 2015a. Mandibular and dental characteristics of Late Triassic mammaliaform *Haramiyavia* and their ramifications for basal mammal evolution. *Proceedings of the National Academy of Sciences* 112: E7101–E7109.

Luo Z-X, Meng Q-J, Ji Q, Liu D, Zhang Y-G, Neander AI. 2015b. Evolutionary development in basal mammaliaforms as revealed by a docodontan. *Science* 347: 760–764.

Luo Z-X, Meng Q-J, Grossnickle DM, Liu D, Zhang Y-G, Neander AI, Ji Q. 2017. New evidence for mammaliaform ear evolution and feeding adaptation in a Jurassic ecosystem. *Nature* 548: 326–329.

Lyckegaard A., Johnson G., Tafforeau P. 2011. Correction of ring artifacts in X-ray tomographic images. *International Journal of Tomography and Statistics* 18: 1–9.

Martin T. 2005. Postcranial anatomy of *Haldanodon exspectatus* (Mammalia, Docodonta) from the Late Jurassic (Kimmeridgian) of Portugal and its bearing for mammalian evolution. *Zoological Journal of the Linnean Society* 145: 219–248.

Martin T. 2006. Early mammalian evolutionary experiments. *Science* 311: 1109–1110.

Martin T. 2008. Mesozoic mammals – early mammalian diversity and ecomorphological adaptations. In: Zachos FE, Asher AJ, eds. *Handbook of Zoology, Mammalia, Mammalian Evolution, Diversity and Systematics*. Berlin: De Gruyter, 199-299.

Martin T, Averianov AO, Pfretzschner H-U. 2010. Mammals from the Late Jurassic Qigu Formation in the Southern Junggar Basin, Xinjiang, Northwest China. *Palaeobiodiversity and Palaeoenvironment* 90: 295–319.

Maschenko EN, Lopatin AV, Voronkevich AV. 2002. A new genus of the tegotheriid docodonts (Docodonta, Tegotheriidae) from the Early Cretaceous of West Siberia. *Russian Journal of Theriology* 1: 75–81.

Meng Q-J, Ji Q, Zhang Y-G, Liu D, Grossnickle DM, Luo Z-X. 2015. An arboreal docodont from the Jurassic and mammaliaform ecological diversification. *Science* 347: 764–768.

Mirone A, Brun E, Gouillart E, Tafforeau P, Kieffer J. 2014. The PyHST2 hybrid distributed code for high speed tomographic reconstruction with iterative reconstruction and a priori knowledge capabilities. *Nuclear Instruments and Methods in Physics Research Section B: Beam Interactions with Materials and Atoms* 324: 41–48.

Morton N, Hudson JD. 1995. Field guide to the Jurassic of the Isles of Raasay and Skye, Inner Hebrides, NW Scotland. In: Taylor PD, ed. *Field Geology of the British Jurassic*. London: Geological Society, 209–280.

Paganin D., Mayo S., Gureyev T.E., Miller P.R.& Wilkins S.W. 2002. Simultaneous phase and amplitude extraction from a single defocused image of a homogeneous object. *Journal of Microscopy* 206: 33–40.

Panciroli E, Benson RBJ, Walsh S. 2017a. The dentary of *Wareolestes rex* (Megazostrodontidae): a new specimen from Scotland and implications for morganucodontan tooth replacement. *Papers in Palaeontology* 3: 373–386.

Panciroli E, Walsh S, Fraser N, Brusatte SL, Corfe I. 2017b. A reassessment of the postcanine dentition and systematics of the tritylodontid *Stereognathus* (Cynodontia,

Tritylodontidae, Mammaliamorpha), from the Middle Jurassic of the UK. *Journal of Vertebrate Paleontology* 37: 373–386.

Panciroli E, Schultz JA, Luo Z-X. 2018a. Morphology of the petrosal and stapes of *Borealestes* (Mammaliaformes, Docodonta) from the Middle Jurassic of Skye, Scotland. *Papers in Palaeontology* 5: 139–156.

Panciroli E, Benson RBJ, Butler RJ. 2018b. New partial dentaries of *Palaeoxonodon ooliticus* (Mammalia, Amphitheriidae) from Scotland, and posterior dentary morphology in stem cladotherians. *Acta Palaeontologica Polonica* 63: 197–206.

Panciroli E, Benson RBJ, Luo Z-X. 2019. The mandible and dentition of *Borealestes serendipitus* (Docodonta) from the Middle Jurassic of Skye, Scotland. *Journal of Vertebrate Paleontology* 39: p.e1621884.

Panciroli E, Benson RBJ, Walsh S, Butler RJ, Castro TA, Jones MEH, Evans SE. 2020. Diverse vertebrate assemblage of the Kilmaluag Formation (Bathonian, Middle Jurassic) of Skye, Scotland. *Earth and Environmental Science Transactions of the Royal Society of Edinburgh* (accepted).

Rees J, Underwood CJ. 2005. Hybodont sharks from the Middle Jurassic of the Inner Hebrides, Scotland. *Earth and Environmental Science Transactions of the Royal Society of Edinburgh* 96: 351–363.

Rougier GW, Sheth AS, Carpenter K, Appella-Guisafre L, Davis BM. 2015. A new species of *Docodon* (Mammaliaformes, Docodonta) from the Upper Jurassic Morrison Formation and a

reassessment of selected craniodental characters in basal mammaliaforms. *Journal of Mammalian Evolution* 22: 1–16.

Rowe T. 1988. Definition, diagnosis and origin of Mammalia. *Journal of Vertebrate Paleontology* 8: 241–264.

Rowe TB, Macrini TE, Luo Z-X. 2011. Fossil evidence on origin of the mammalian brain. *Science*. 332: 955–957.

Ruf I, Luo Z-X, Martin T. 2013. Reinvestigation of the basicranium of *Haldanodon exspectatus* (Mammaliaformes, Docodonta). *Journal of Vertebrate Paleontology* 33: 382–400.

Schultz JA, Bhullar BAS, Luo Z-X. 2017. Re-examination of the Jurassic mammaliaform *Docodon victor* by computed tomography and occlusal functional analysis. *Journal of Mammalian Evolution* 26: 9–38.

Sigogneau-Russell D. 2003. Docodonts from the British Mesozoic. *Acta Palaeontologica Polonica* 48: 357–374.

Sigogneau-Russell D, Hahn R. 1995. Reassessment of the Late Triassic symmetrodont mammal *Woutersia*. *Acta Palaeontologica Polonica* 40: 245–260.

Simpson GG. 1929. American Mesozoic Mammalia. *Memoirs of the Peabody Museum of Yale University* 3: 1–235.

Sues HD, Jenkins Jr FA. 2006. The postcranial skeleton of *Kayentatherium wellesi* from the Lower Jurassic Kayenta Formation of Arizona and the phylogenetic significance of postcranial

features in tritylodontid cynodonts. In: Carrano MT, ed. *Amniote Paleobiology: Perspectives on the Evolution of Mammals, Birds, and Reptiles*. Chicago: University of Chicago Press, 114–152.

Swofford, D.L. 2003. PAUP*. Phylogenetic Analysis Using Parsimony (*and Other Methods). Version 4. Sinauer Associates, Sunderland, Massachusetts.

Wakefield MI. 1995. Ostracod biostratinomy at lagoonal shorelines: examples from the Great Estuarine Group, Middle Jurassic, Scotland. *Proceedings of the Geologists' Association* 106: 211–218.

Waldman M, Evans SE. 1994. Lepidosauromorph reptiles from the Middle Jurassic of Skye. *Zoological Journal of the Linnean Society* 112: 135–150.

Waldman M, Savage RJG. 1972. The first Jurassic mammal from Scotland. *Journal of the Geological Society of London* 128: 119–125.

Wible JR, Hopson JA. 1993. Basicranial evidence for early mammal phylogeny. In: Szalay FS, Novacek MJ, McKenna MC, eds. *Mammal phylogeny: Mesozoic differentiation, multituberculates, monotremes, early therians and marsupials*. New York: Springer, 45–62.

Wible JR, Burrows AM. 2016. Does the Jurassic *Agilodocodon* (Mammaliaformes, Docodonta) have any exudativorous dental features? *Palaeontologia Polonica* **67**: 289–299.

Wills S, Barrett PM, Walker A. 2014. New dinosaur and crocodylomorph material from the Middle Jurassic (Bathonian) Kilmaluag Formation, Skye, Scotland. *Scottish Journal of Geology* **50**: 183–190.

Zhou CF, Wu S, Martin T, Luo Z-X. 2013. A Jurassic mammaliaform and the earliest mammalian evolutionary adaptations. *Nature* **500**: 163–167.

Zhou C-F, Bhullar, B-AS, Neander AI, Martin T. Luo Z-X. 2019. New Jurassic mammaliaform sheds light on early evolution of mammal-like hyoid bones. *Science* **365**: 276–279.

FIGURE LEGENDS

Figure 1: The stratigraphy of the Great Estuarine Group, and location of type locality of *Borealestes serendipitus* NMS G.1992.141.1 and *Borealestes cuillinensis* sp. nov. NMS G.2020.4.1.1, Cladach a'Ghlinne near Elgol.

Figure 2: *Borealestes serendipitus* cranial elements (NMS G.1992.47.121.1) Visualisation from synchrotron μCT data. A, NMS G.1992.47.121.1, showing location of cranial elements; B, digital rendering of surface of NMS G.1992.47.121.1; C, digital rendering of surface of NMS G.1992.47.121.1 with matrix semitransparent, showing skeletal elements within the block. Scale bar equals 10 mm.

Figure 3: *Borealestes cuillinensis* sp. nov. cranial elements (NMS G.2020.4.1.1 parts AA and BB) visualisation from μCT data. A, digital rendering of surface of NMS G.2020.4.1.1; B, digital rendering of NMS G.2020.4.1.1 with matrix semitransparent, showing cranial skeletal elements within the block. Scale bar equals 10 mm.

Figure 4: Phylogeny of Docodonta based on updated phylogenetic analysis. Strict consensus of six trees of 131 steps resulting from parsimony analysis of data matrix for docodontans and outgroups as in Panciroli *et al.* (2019), with the addition of *Borealestes cuillinensis* and revision

of *Dobunnodon* (=*'Borealestes' mussettae*). First-to-last appearances represented by black bars (see Supplementary). Nodes uniting taxa do not imply divergence times.

Figure 5: Diagnostic dental features of *Borealestes* species, and *Dobunnodon* gen. nov. A, *Borealestes serendipitus*: A1, NMS G.1992.47.121.1 left M3 (mirrored) in occlusal view alongside diagrammatic illustration; A2, holotype BRSUG 20570 right m2 (mirrored) in occlusal view, cusps only, alongside diagrammatic illustration; and A3, BRSUG 20570 right m2 (mirrored) crests only; A4 BRSUG 20570 right m2 (mirrored) in lingual view alongside diagrammatic illustration. B, *Borealestes cuillinensis*: B1, NMS G.2020.4.1.1 right M3 in occlusal view alongside diagrammatic illustration; B2, NHMUK PV M46871 left upper molar in occlusal view (mirrored) with cusps marked; B3, NMS G.2020.4.1.1 m2 in occlusal view; and B4 NMS G.2020.4.1.1 m2 in lingual view with cusps alongside diagrammatic illustration. C, *Dobunnodon mussettae* gen. nov.: C1, holotype NHMUK PV M46495 lower right molar in occlusal view with crests and diagrammatic illustration below; C2, holotype NHMUK PV M46495 mirrored for comparison and diagrammatic illustration below, C3, holotype NHMUK PV M46495 lingual view with crests and diagrammatic illustration below; C4, holotype NHMUK PV M46495 mirrored for comparison. A and C adapted from Panciroli *et al*. (2019). Darker grey areas indicate broken surfaces. Scale bars equal 1 mm.

Figure 6: Dentition of *Borealestes serendipitus* and *Borealestes cuillinensis* for comparison. A and C. *Borealestes serendipitus* upper dentition of NMS G.1992.47.121.1 and lower dentition of NMS G.1992.47.121.3 (C mirrored for comparison). B and D *Borealestes cuillinensis* NMS G.2020.4.1.1. Scale bars equal 1 mm.

Figure 7: Diagnostic mandibular features of *Borealestes* species. A1 and A2 dentaries belong to *Borealestes serendipitus*, showing diagnostic features of Meckel's sulcus and mandibular

symphysis. Bottom dentary B, belongs to *Borealestes cuillinensis*. Shows diagnostic features of Meckel's sulcus and mandibular symphysis. Scale bar equals 1 mm, scale same throughout.

Figure 8: Skull reconstruction of *Borealestes serendipitus* in lateral (top) dorsal (middle) and ventral (bottom) views. Green shaded areas represented in specimen NMS G.1992.47.121.1 and associated material. Dotted lines indicate unrepresented areas where boundaries unknown. 1 Premaxilla; 2 anterior nasal foramina; 3 maxilla; 4 infraorbital foramen; 5 posterior nasal foramen; 6 lacrimal; 7 nasal; 8 lacrimal foramen; 9 zygomatic process of lacrimal; 10 jugal (not known); 11 infraorbital foramen; 12 frontal; 13 parietal; 14 interparietal suture; 15 sagittal crest; 16 squamosal; 17 dorsal flange of squamosal; 18 postparietal; 19 occipital condyles; 20 midline ridge of postparietal; 21 postparietal foramina; 22 septomaxilla; 23 anterior projection of nasal; 24 internarial bar; 25 anterior premaxillary foramen; 26 incisive foramen; 27 palatal posterior salient of premaxilla; 28 greater palatine foramen; 29 palatal process (not known); 30 glenoid fossa; 31 external auditory meatus; 32 fenestra vestibuli; 33 pars cochlearis; 34 orbital area (not known); 35 basicranium (not known); 36 pterygoid and basicranium (not known); 37 primary palate (not known); 38 I3 foramen; 39 posterior projection of premaxilla into incisive foramen; 40 coronoid process; 41 nuchal crest; 42 angular process of dentary; 43 masseteric foramen; 44 dentary; 45 mental foramen; 46 anterior premaxillary foramen. Scale bar equals 5 mm.

Figure 9: Skull reconstruction of *Borealestes cuillinensis* in lateral (top) dorsal (middle) and ventral (bottom) views. Blue shaded areas represented in specimen NMS G.2020.4.1.1. Dotted lines indicate unrepresented areas where boundaries unknown. 1 Premaxilla; 2 anterior nasal foramina; 3 maxilla; 4 infraorbital foramen; 5 posterior nasal foramen (not known); 6 lacrimal; 7 nasal; 8 lacrimal foramen; 9 zygomatic process of lacrimal; 10 jugal (not known); 11 infraorbital foramen (not known); 12 frontal (not known); 13 parietal (not known); 14 interparietal suture; 15 sagittal crest (not known); 16 squamosal; 17 dorsal flange of squamosal; 18 postparietal (not known); 19 occipital condyles; 20 midline ridge of postparietal; 21 postparietal foramina; 22

septomaxilla; 23 anterior projection of nasal; 24 internarial bar; 25 anterior premaxillary foramen (not known); 26 incisive foramen; 27 palatal posterior salient of premaxilla (not known); 28 greater palatine foramen; 29 palatal process (not known); 30 glenoid fossa; 31 external auditory meatus; 32 fenestra vestibuli; 33 pars cochlearis; 34 orbital area (not known); 35 basicranium known); 36 pterygoid and basicranium (not known); 37 primary palate (not known); 38 I3 foramen (not known); 39 posterior projection of premaxilla into incisive foramen (not known); 40 coronoid process; 41 nuchal crest (not known); 42 angular process of dentary; 43 masseteric foramen; 44 dentary; 45 mental foramen; 46 anterior premaxillary foramen. Scale bar equals 5 mm.

Figure 10: *Borealestes cuillinensis* sp. nov. (holotype, NMS G.2020.4.1.1) left mandible, A, occlusal view; B, lateral view; C, lingual view. Arrows indicate anterior direction. The triangle indicates the alignment of the ultimate molar to the coronoid process. Angular process broken during preparation and replaced digitally, broken lines indicate missing piece of process. Scale bar equals 1 mm, scale same throughout.

Figure 11: *Borealestes cuillinensis* (holotype, NMS G.2020.4.1.1) anterior part of right dentary and right premaxilla. A, right dentary: A1, right lateral view; A2, lingual view; A3, occlusal view. B, fragment of right premaxilla: B1, right lateral view; B2, occlusal view. Arrows indicate anterior direction. Scale bar equals 1 mm, scale same throughout.

Figure 12: *Borealestes serendipitus* skull elements. Premaxillae with incisors and anterior nasal part (NMS G.1992.47.121.4), with diagrammatic illustrations; A1, left lateral view; A2, right lateral view; A3, anterior view; A4, dorsal view; A5, ventral view; A6, semitransparent digital rendering of reconstructed premaxillae and incisors, showing path of premaxillary canal. B, Nasal anterior part: B1 ventral view; B2, medial view; B3, dorsal view; B4, left lateral view. Arrows indicate anterior direction. Dark grey areas on diagrammatic illustrations indicate broken surfaces. Scale bar equals 1 mm, scale same throughout.

Figure 13: *Borealestes serendipitus* (NMS G.1992.47.121.1) palatal portion of cranium and right lacrimal. A, ventral view; A2, right lateral view with diagrammatic illustration below; B, right lacrimal (see also Fig. 13); B1, right posterolateral view; B2, dorsal view; B3, medial view; B4 right lateral view. Arrows indicate anterior direction. Dark grey areas on diagrammatic illustrations indicate broken surfaces. Scale bar equals 1 mm, scale same throughout.

Figure 14: *Borealestes serendipitus* (NMS G.1992.47.121.1) palatal portion of cranium and left lacrimal. A, virtual slice from synchrotron μCT showing cross-section of palate; B, dorsal view with diagrammatic illustration below; C, left lacrimal: C1, dorsal view; C2, left lateral view; C3 medial view; C4, ventral view. Arrows indicate anterior direction. Dark grey areas on diagrammatic illustrations indicate broken surfaces. Scale bar equals 1 mm, scale same throughout.

Figure 15: *Borealestes cuillinensis* (holotype, NMS G.2020.4.1.1) left maxilla. A, left maxilla with diagrammatic illustrations: A1, left lateral view; A2, occlusal view; A3, dorsal/endocranial view. Arrows indicate anterior direction. Dark grey areas on diagrammatic illustrations indicate broken surfaces. Scale bar equals 1 mm, scale same throughout.

Figure 16: *Borealestes cuillinensis* (holotype NMS G.2020.4.1.1) right maxilla and palatal process. A, posterior portion of right maxilla: A1, right lateral view; A2, occlusal view; A3, dorsal/endocranial view. B, palatal process of right maxilla: B1, dorsal/endocranial view; B2, ventral/palatal view; B3, medial view. Arrows indicate anterior direction. Scale bar equals 1 mm, scale same throughout.

Figure 17: *Borealestes cuillinensis* (holotype, NMS G.2020.4.1.1) nasals and ?lacrimal. A, right nasals: A, ventral/endocranial view; A2, dorsal view; A3, medial view. B, right ?nasal: B1, dorsal view; B2, lateral view; B3, medial/endocranial view. Arrows indicate anterior direction. Scale bar equals 1 mm, scale same throughout.

Figure 18: *Borealestes cuillinensis* (holotype, NMS G.2020.4.1.1) right lacrimal and diagrammatic illustrations: A1, right lateral view; C2, endocranial view; C3, dorsal view. Arrows indicate anterior direction. Dark grey areas on diagrammatic illustrations indicate broken surfaces. Scale bar equals 1 mm, scale same throughout.

Figure 19: *Borealestes serendipitus* (NMS G.1992.47.121.1) elements of cranium. A, left frontal: A1, synchrotron μCT slice showing cross section through left frontal; A2, ventral view; A3, dorsal view; A4, medial view; A5, left lateral view. B the left squamosal, reconstructed (originally in two misaligned pieces): B1, ventral view; B2, dorsal view; C, the occipital condyles. D, postparietal: D1, posterodorsal view; D2, virtual slice from synchrotron μCT showing cross section through postparietal; D3, anterior/endocranial view; D4, anteroventral view. Arrows indicate anterior direction. Scale bar equals 1 mm, scale same throughout.

Figure 20: *Borealestes serendipitus* (NMS G.1992.47.121.1) left parietal. A, endocranial/ventral view; B, dorsal view; C, medial view; D, left lateral view. Arrows indicate anterior direction. Scale bar equals 1 mm, scale same throughout.

Figure 21: *Borealestes cuillinensis* (holotype, NMS G.2020.4.1.1) squamosal and occipitals. A, the right squamosal: A1, ventral view; A2, dorsal view; A3, medioventral view; A4, laterodorsal view; A5, right lateral view. B, the anterior tip of the left squamosal of (zygomatic process): B1, dorsal view; B2, ventral view; B3, lateral view. C, the occipital condyles: C1, condyles as preserved in specimen; C2, condyles reconstructed. Arrows indicate anterior direction. Scale bar equals 1 mm, scale same throughout.

Table 1: List of parameters used for XCT acquisition of the specimens. N. of Proj = number of projections; fr. av. = frame averaging; UoB = University of Bristol; UoE = University of Edinburgh. Asterisk indicated data is missing.

Specimen number	CT system	Voxel size (µm)	N. of Proj.	Filter (mm)	kV	µA	Power W	Exp. (s)	Fr. av.
NMS G.2020.4.1.1 (part AA)	Nikon XTH 225 ST (UoB)	22.14	2201	Cu 0.5	180	111	19.98	0.708	4
NMS G.2020.4.1.1 (partBB)	Nikon XTH 225 ST (UoB)	20.05	3141	none	130	154	20.02	0.5	4
NMS G.1992.47.121.1	ESRF	6.15	6000	Al 5.6 Cu 5.6 W 0.5	201			0.3	
NMS G.1992.47.121.3	Nikon XTH 225 ST (UoB)	12.77	*	*	*	*	*	*	*
NMS G.1992.47.121.4	in-house built µCT (UoE)	6.43	*	none	*	*	*	*	*
NMS G.1992.47.121.2	in-house built µCT (UoE)	8.9	2000	Al 0.8	70	40	2.8	2	n.a

Table 2: Measurements of the dentition of *Borealestes* and *Dobunnodon.* All measurements in mm. Methodology as for Panciroli *et al.* (2019)

	(mm)		c/ C	pm1/ PM1	pm2/ PM2	pm3/ PM3	pm4/ PM4	pm5/ PM5	m1/ M1	m2/M 2	m3/ M3	m4/ M4	m5/ M5
Lower tooth row													
NMS G.1992.47.121.3	Length	d to b	-	-	0.84	1.04	1.15	1.25	1.38	1.47	1.5	1.33	0.93
		df to e	-	-	-	-	-	-	1.35	1.41	1.49	1.31	0.85
	Width	cross c	-	*0.36*	0.39	0.42	0.46	0.48	0.79	0.89	0.97	0.78	0.43
		cross g	-	-	-	-	-	-	0.69	0.83	0.92	0.83	0.57
NMS G.2020.4.1.1 (*B. cuillinensis*) (ant right dentary)	Length	d to b	*0.73*	0.63	0.74	0.95	1.10	1.1	1.32	1.42	-	-	-
		df to e	-	-	-	-	-	-	1.4	1.33	-	-	-
	Width	cross c	0.43	0.34	0.34	0.32	0.47	0.48	0.56	0.64	-	-	-
		cross g	-	-	-	-	-	-	0.71	0.68	-	-	-
NMS G.2020.4.1.1 (*B. cuillinensis*) (post left dentary)	Length	d to b	-	-	-	-	*1.05*	1.11.	1.3	1.36	1.2	1.04	0.7
		df to e	-	-	-	-	-	-	1.3	1.36	1.25	1.07	0.63
	Width	cross c					0.44	0.43	0.83	0.86	0.90	0.62	0.42
		cross g					-	-	0.71	0.83	0.84	0.7	0.48
NHMUK PV M46495 (*Dobunnodon. mussettae*)	Length	d to b	-	-	-	-	-	-	1.51	-	-	-	-
		df to e	-	-	-	-	-	-	1.57	-	-	-	-
	Width	cross c	-	-	-	-	-	-	0.67	-	-	-	-
		cross g	-	-	-	-	-	-	0.58	-	-	-	-
Upper tooth row													
NMS G.1992.47.121.1 (*B. cuillinensis*)	Right tooth row	Length	buccal	-	-	-	-	-	-	-	1.6	1.17	-
			lingual	-	-	-	-	-	0.81	0.98	0.95	0.7	-
		Width		-	-	-	-	-	*1.4*	1.6	1.67	1.41	-
	Left tooth row	Length	buccal	-	-	-	-	-	-	-	1.42	1.18	-

			lingual	-	-	-	-	-	0.77	0.9	0.93	0.7	-
		Width		-	-	-	-	-	1.77	1.63	1.39	1.77	-
NMS G.2020.4.1.1 (*B. cuillinensis*)	Right tooth row	Length	buccal	-	-	-	0.99	1.02	1.5	1.38	1.2	0.9	-
			lingual	-	-	-	-	-	0.74	0.84	0.71	0.63	-
		Width		-	-	-	0.58	0.75	*1.51*	1.66	1.58	1.1	-
	Left tooth row	Length	buccal	-	-	1.09	*1.01*	-	-	1.28	1.46	0.97	-
			lingual	-	-	-	-	-	-	0.9	0.83	0.8	-
		Width		-	-	-	-	-	-	1.58	1.58	1.06	

Table 3: Measurements of dentaries and maxillae of *Borealestes*.

Specimen number	Element	Length (mm)	Width (mm)
NMS G.1992.47.121.1	Right dentary	22.98	0.97 (ventral to m3)
	Left maxilla (partial)	4.15	-
	Right maxilla (partial)	4.67	-
NMS G.2020.4.1.1	Right dentary (partial)	9.01	1.01 (ventral to m2)
	Left dentary (partial)	16.4	0.98 (ventral to m3)
	Left maxilla (partial)	7.91	-

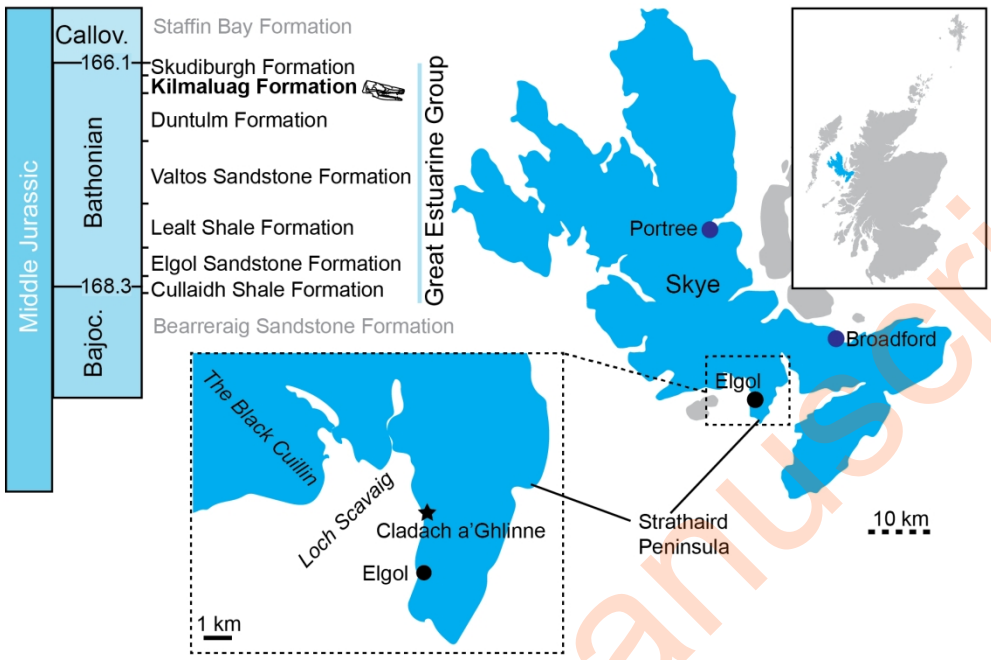

Figure 1: The stratigraphy of the Great Estuarine Group, and location of type locality of *Borealestes serendipitus* NMS G.1992.141.1 and *Borealestes cuillinensis* sp. nov. NMS G.2020.4.1.1, Cladach a'Ghlinne near Elgol.

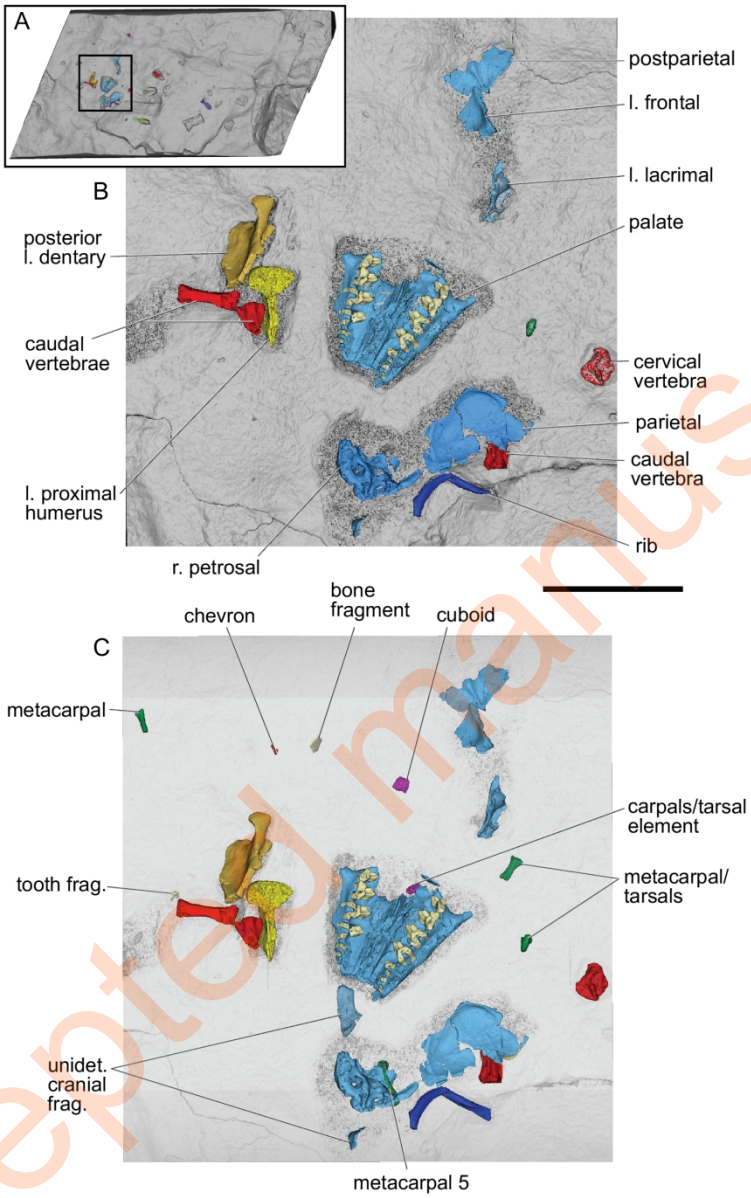

Figure 2: *Borealestes serendipitus* cranial elements (NMS G.1992.47.121.1) Visualisation from synchrotron μCT data. A, NMS G.1992.47.121.1, showing location of cranial elements; B, digital rendering of surface of NMS G.1992.47.121.1; C, digital rendering of surface of NMS G.1992.47.121.1 with matrix semitransparent, showing skeletal elements within the block. Scale bar equals 10 mm.

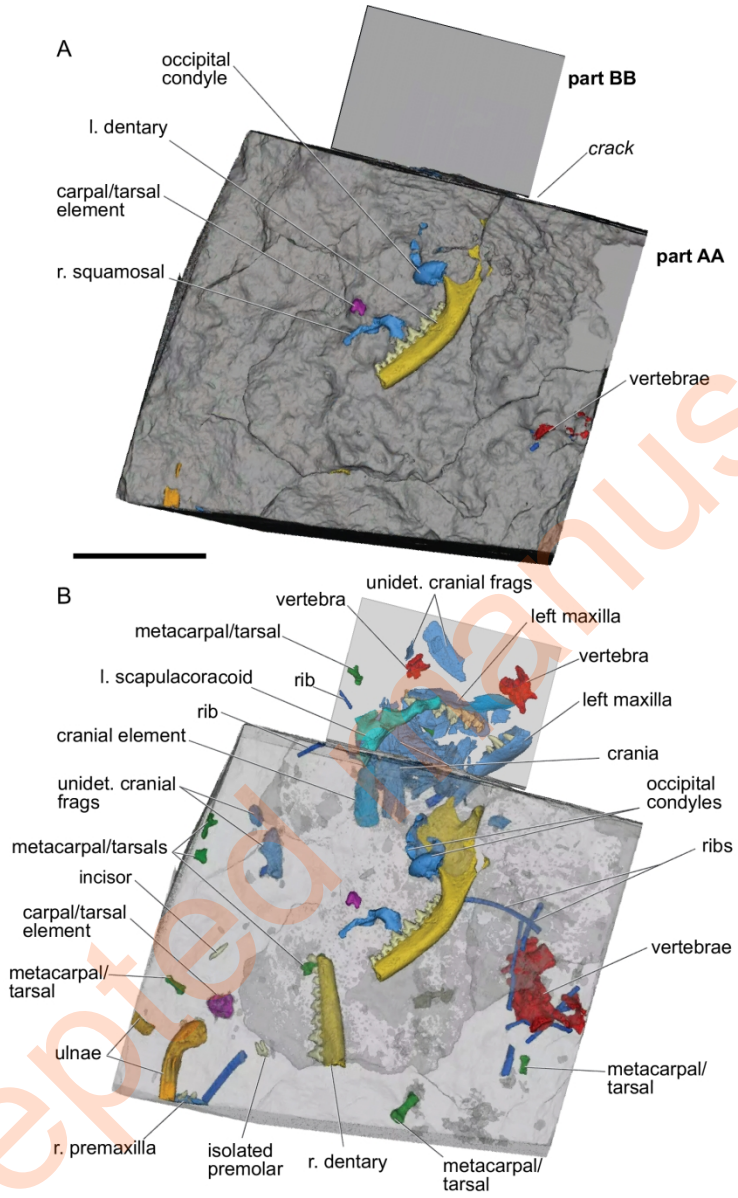

Figure 3: *Borealestes cuillinensis* sp. nov. cranial elements (NMS G.2020.4.1.1 parts AA and BB) visualisation from µCT data. A, digital rendering of surface of NMS G.2020.4.1.1; B, digital rendering of NMS G.2020.4.1.1 with matrix semitransparent, showing cranial skeletal elements within the block. Scale bar equals 10 mm.

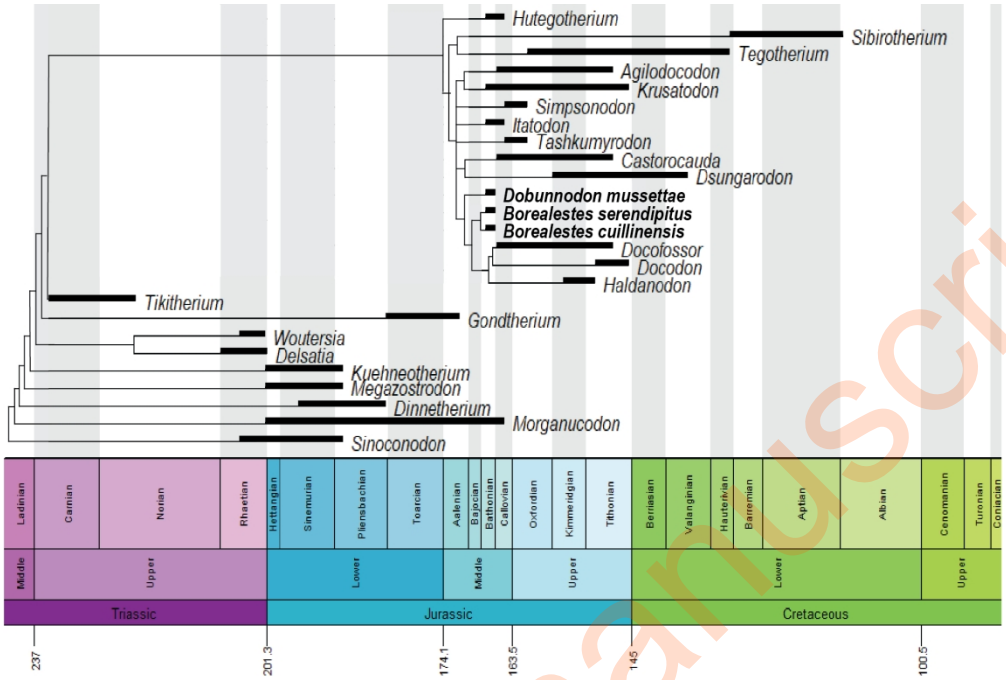

Figure 4: Phylogeny of Docodonta based on updated phylogenetic analysis. Strict consensus of six trees of 131 steps resulting from parsimony analysis of data matrix for docodontans and outgroups as in Panciroli et al. (2019), with the addition of *Borealestes cuillinensis* and revision of Dobunnodon (=*'Borealestes' mussettae*). First-to-last appearances represented by black bars (see Supplementary). Nodes uniting taxa do not imply divergence times.

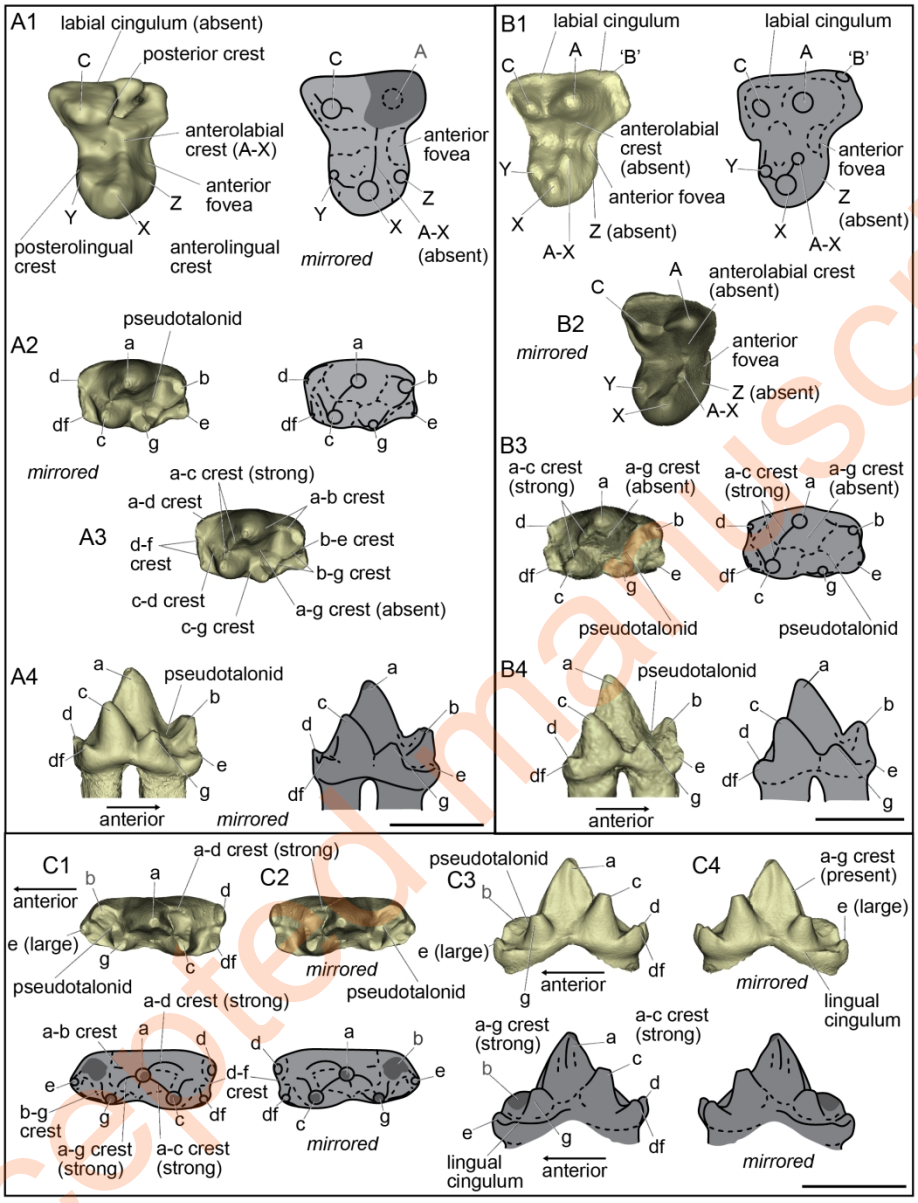

Figure 5: Diagnostic dental features of *Borealestes* species, and *Dobunnodon* gen. nov. A, *Borealestes serendipitus*: A1, NMS G.1992.47.121.1 left M3 (mirrored) in occlusal view alongside diagrammatic illustration; A2, holotype BRSUG 20570 right m2 (mirrored) in occlusal view, cusps only, alongside diagrammatic illustration; and A3, BRSUG 20570 right m2 (mirrored) crests only; A4 BRSUG 20570 right m2 (mirrored) in lingual view alongside diagrammatic illustration. B, *Borealestes cuillinensis*: B1, NMS G.2020.4.1.1 right M3 in occlusal view alongside diagrammatic illustration; B2, NHMUK PV M46871 left upper molar in occlusal view (mirrored) with cusps marked; B3, NMS G.2020.4.1.1 m2 in occlusal view; and B4 NMS G.2020.4.1.1 m2 in lingual view with cusps alongside diagrammatic illustration. C, *Dobunnodon mussettae* gen. nov.: C1, holotype NHMUK PV M46495 lower right molar in occlusal view with crests and diagrammatic illustration below; C2, holotype NHMUK PV M46495 mirrored for comparison and diagrammatic illustration below, C3, holotype NHMUK PV M46495 lingual view with crests and diagrammatic illustration below; C4, holotype NHMUK PV M46495 mirrored for comparison. A and C adapted from Panciroli et al. (2019). Darker grey areas indicate broken surfaces. Scale bars equal 1 mm.

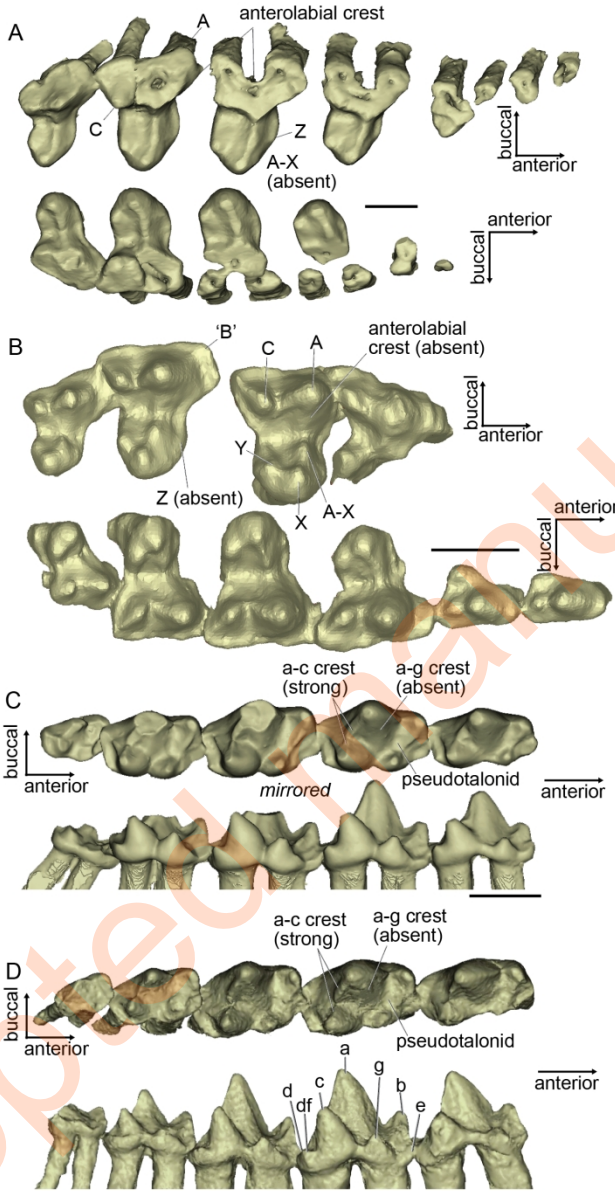

Figure 6: Dentition of *Borealestes serendipitus* and *Borealestes cuillinensis* for comparison. A and C. *Borealestes serendipitus* upper dentition of NMS G.1992.47.121.1 and lower dentition of NMS G.1992.47.121.3 (C mirrored for comparison). B and D *Borealestes cuillinensis* NMS G.2020.4.1.1. Scale bars equal 1 mm.

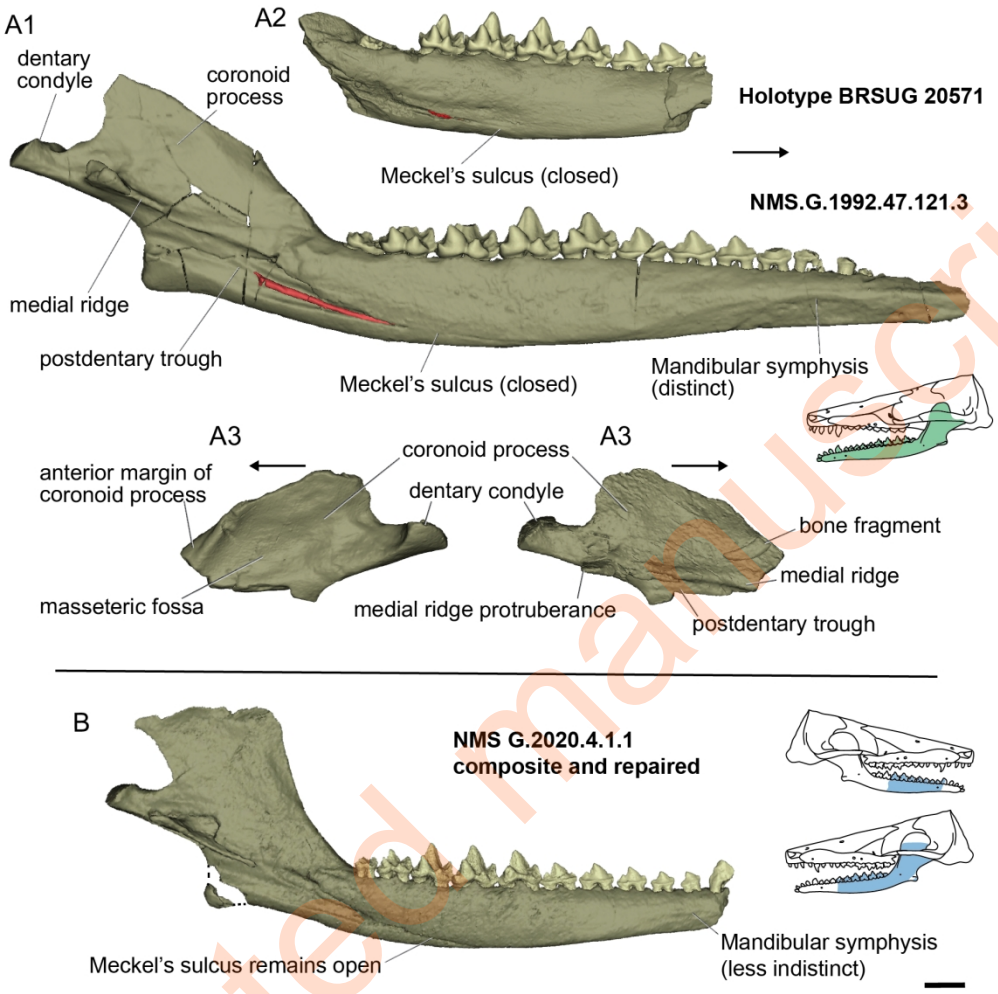

Figure 7: Diagnostic mandibular features of *Borealestes* species. A1 and A2 dentaries belong to *Borealestes serendipitus*, showing diagnostic features of Meckel's sulcus and mandibular symphysis. Bottom dentary B, belongs to *Borealestes cuillinensis*. Shows diagnostic features of Meckel's sulcus and mandibular symphysis. Scale bar equals 1 mm, scale same throughout.

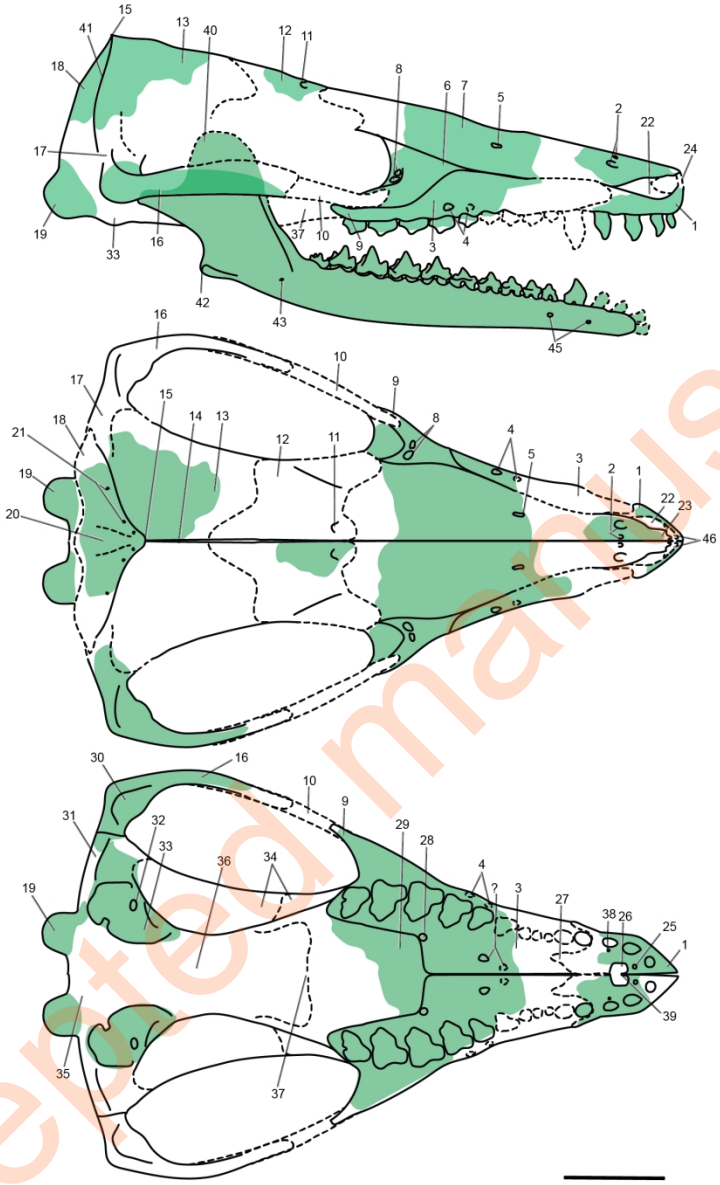

Figure 8: Skull reconstruction of *Borealestes serendipitus* in lateral (top) dorsal (middle) and ventral (bottom) views. Green shaded areas represented in specimen NMS G.1992.47.121.1 and associated material. Dotted lines indicate unrepresented areas where boundaries unknown. 1 Premaxilla; 2 anterior nasal foramina; 3 maxilla; 4 infraorbital foramen; 5 posterior nasal foramen; 6 lacrimal; 7 nasal; 8 lacrimal foramen; 9 zygomatic process of lacrimal; 10 jugal (not known); 11 infraorbital foramen; 12 frontal; 13 parietal; 14 interparietal suture; 15 sagittal crest; 16 squamosal; 17 dorsal flange of squamosal; 18 postparietal; 19 occipital condyles; 20 midline ridge of postparietal; 21 postparietal foramina; 22 septomaxilla; 23 anterior projection of nasal; 24 internarial bar; 25 anterior premaxillary foramen; 26 incisive foramen; 27 palatal posterior salient of premaxilla; 28 greater palatine foramen; 29 palatal process (not known); 30 glenoid fossa; 31 external auditory meatus; 32 fenestra vestibuli; 33 pars cochlearis; 34 orbital area (not known); 35 basicranium (not known); 36 pterygoid and basicranium (not known); 37 primary palate (not known); 38 I3 foramen; 39 posterior projection of premaxilla into incisive foramen; 40 coronoid process; 41 nuchal crest; 42 angular process of dentary; 43 masseteric foramen; 44 dentary; 45 mental foramen; 46 anterior premaxillary foramen. Scale bar equals 5 mm.

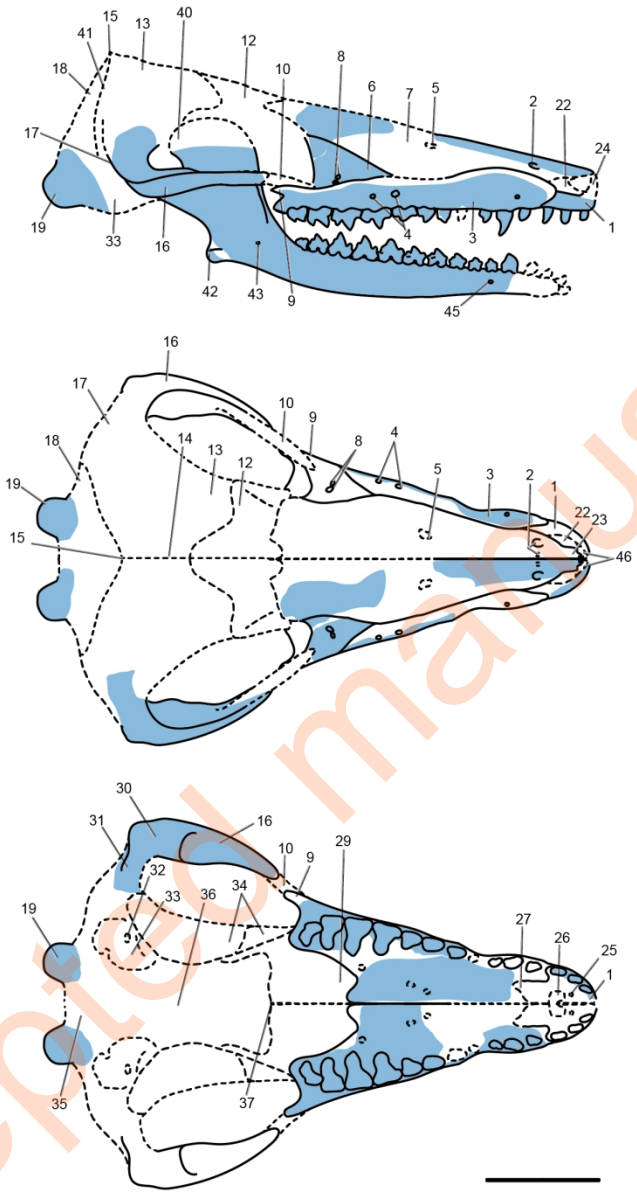

Figure 9: Skull reconstruction of *Borealestes cuillinensis* in lateral (top) dorsal (middle) and ventral (bottom) views. Blue shaded areas represented in specimen NMS G.2020.4.1.1. Dotted lines indicate unrepresented areas where boundaries unknown. 1 Premaxilla; 2 anterior nasal foramina; 3 maxilla; 4 infraorbital foramen; 5 posterior nasal foramen (not known); 6 lacrimal; 7 nasal; 8 lacrimal foramen; 9 zygomatic process of lacrimal; 10 jugal (not known); 11 infraorbital foramen (not known); 12 frontal (not known); 13 parietal (not known); 14 interparietal suture; 15 sagittal crest (not known); 16 squamosal; 17 dorsal flange of squamosal; 18 postparietal (not known); 19 occipital condyles; 20 midline ridge of postparietal; 21 postparietal foramina; 22 septomaxilla; 23 anterior projection of nasal; 24 internarial bar; 25 anterior premaxillary foramen (not known); 26 incisive foramen; 27 palatal posterior salient of premaxilla (not known); 28 greater palatine foramen; 29 palatal process (not known); 30 glenoid fossa; 31 external auditory meatus; 32 fenestra vestibuli; 33 pars cochlearis; 34 orbital area (not known); 35 basicranium known); 36 pterygoid and basicranium (not known); 37 primary palate (not known); 38 I3 foramen (not known); 39 posterior projection of premaxilla into incisive foramen (not known); 40 coronoid process; 41 nuchal crest (not known); 42 angular process of dentary; 43 masseteric foramen; 44 dentary; 45 mental

foramen; 46 anterior premaxillary foramen. Scale bar equals 5 mm.

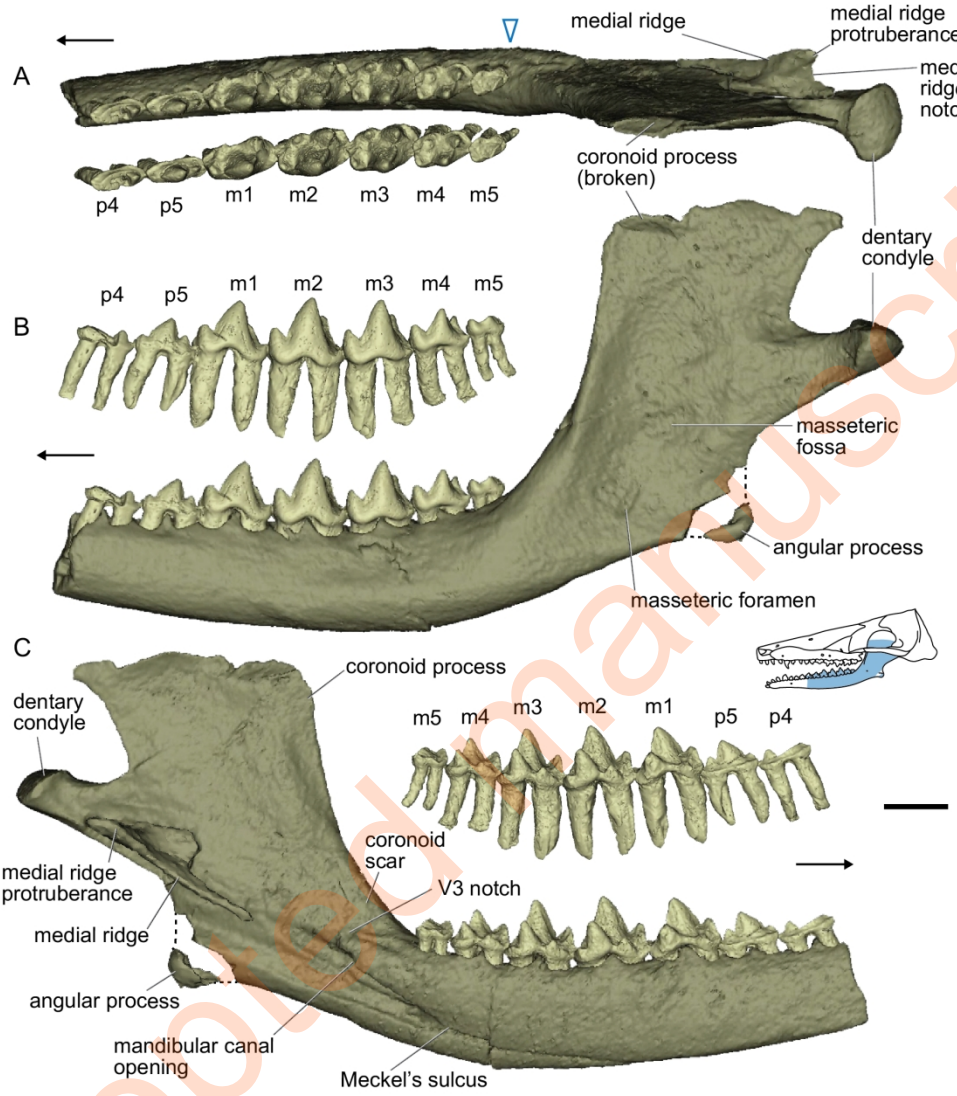

Figure 10: *Borealestes cuillinensis* sp. nov. (holotype, NMS G.2020.4.1.1) left mandible, A, occlusal view; B, lateral view; C, lingual view. Arrows indicate anterior direction. The triangle indicates the alignment of the ultimate molar to the coronoid process. Angular process broken during preparation and replaced digitally, broken lines indicate missing piece of process. Scale bar equals 1 mm, scale same throughout.

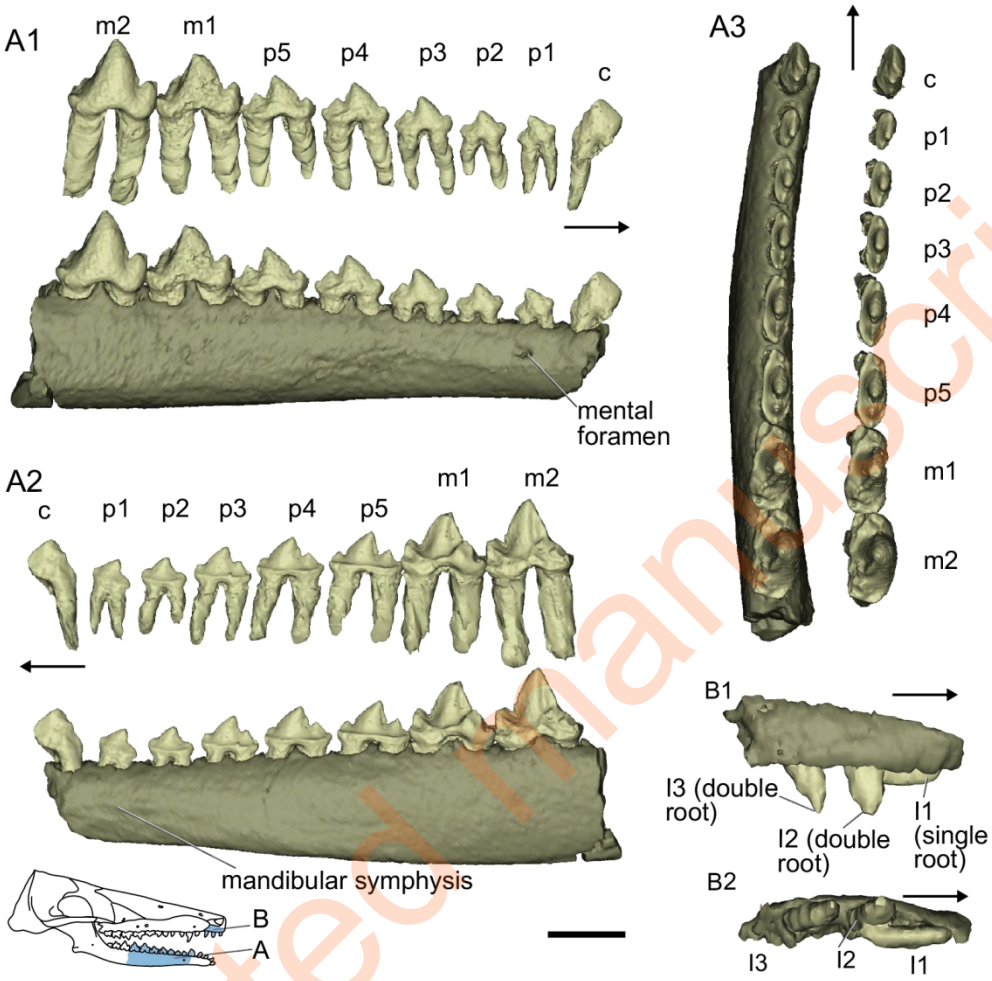

Figure 11: *Borealestes cuillinensis* (holotype, NMS G.2020.4.1.1) anterior part of right dentary and right premaxilla. A, right dentary: A1, right lateral view; A2, lingual view; A3, occlusal view. B, fragment of right premaxilla: B1, right lateral view; B2, occlusal view. Arrows indicate anterior direction. Scale bar equals 1 mm, scale same throughout.

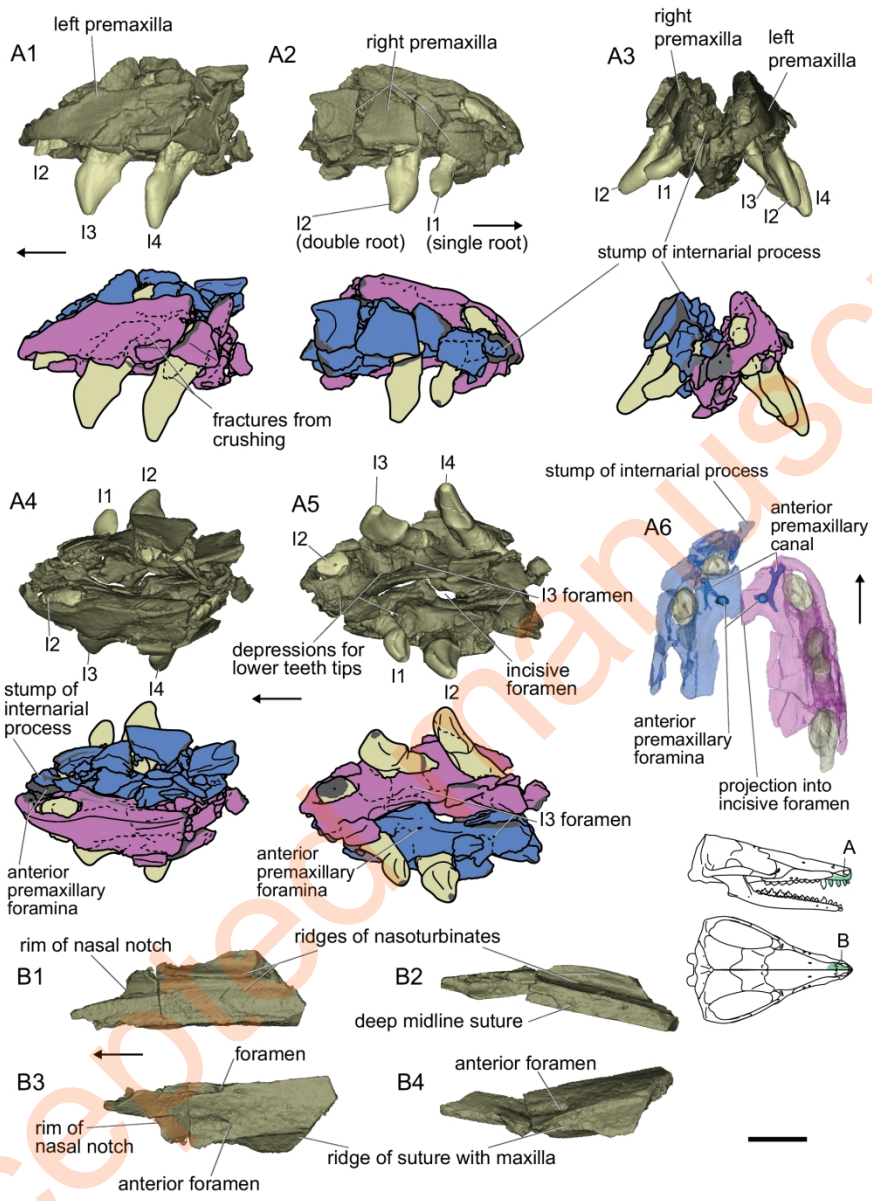

Figure 12: *Borealestes serendipitus* skull elements. Premaxillae with incisors and anterior nasal part (NMS G.1992.47.121.4), with diagrammatic illustrations; A1, left lateral view; A2, right lateral view; A3, anterior view; A4, dorsal view; A5, ventral view; A6, semitransparent digital rendering of reconstructed premaxillae and incisors, showing path of premaxillary canal. B, Nasal anterior part: B1 ventral view; B2, medial view; B3, dorsal view; B4, left lateral view. Arrows indicate anterior direction. Dark grey areas on diagrammatic illustrations indicate broken surfaces. Scale bar equals 1 mm, scale same throughout.

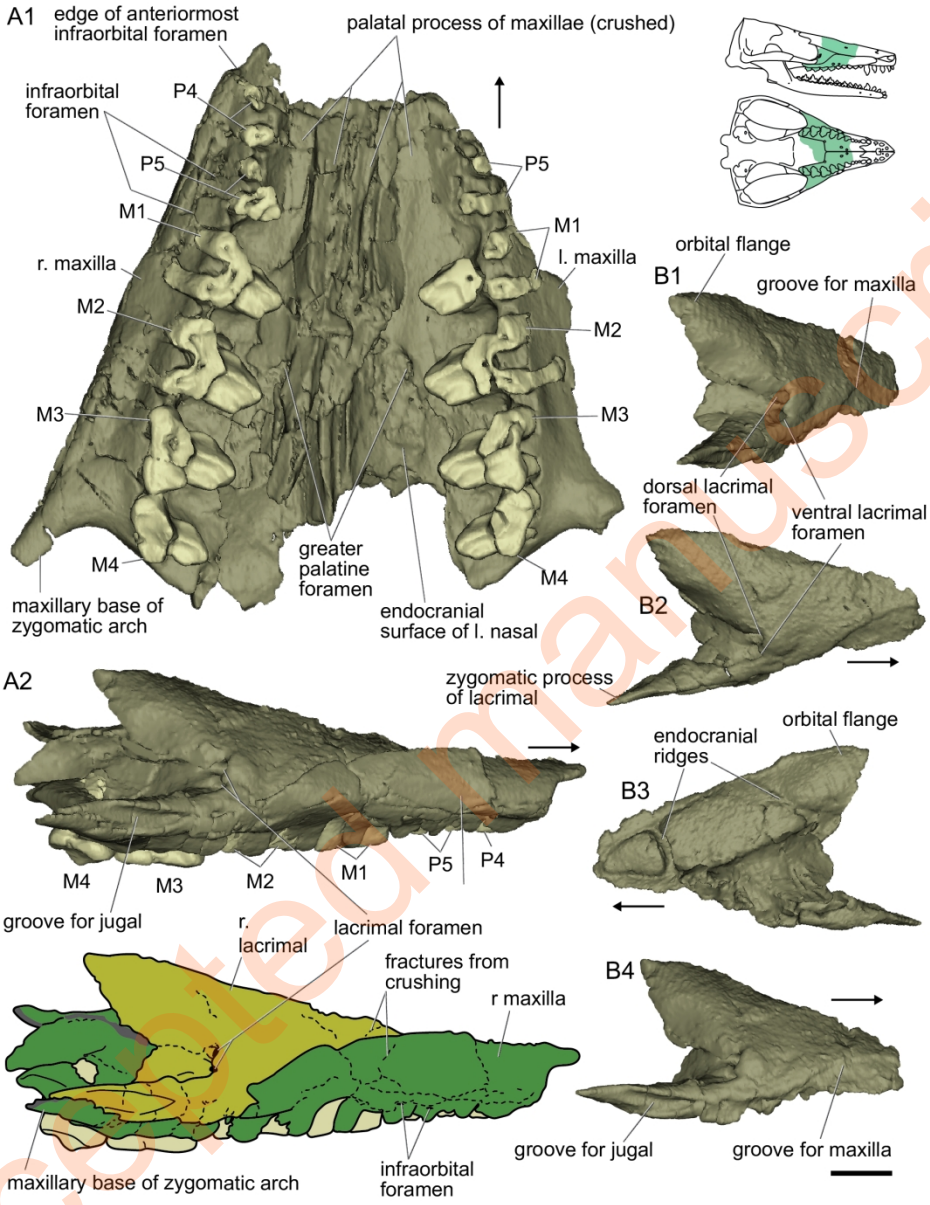

Figure 13: *Borealestes serendipitus* (NMS G.1992.47.121.1) palatal portion of cranium and right lacrimal. A, ventral view; A2, right lateral view with diagrammatic illustration below; B, right lacrimal (see also Fig. 13); B1, right posterolateral view; B2, dorsal view; B3, medial view; B4 right lateral view. Arrows indicate anterior direction. Dark grey areas on diagrammatic illustrations indicate broken surfaces. Scale bar equals 1 mm, scale same throughout.

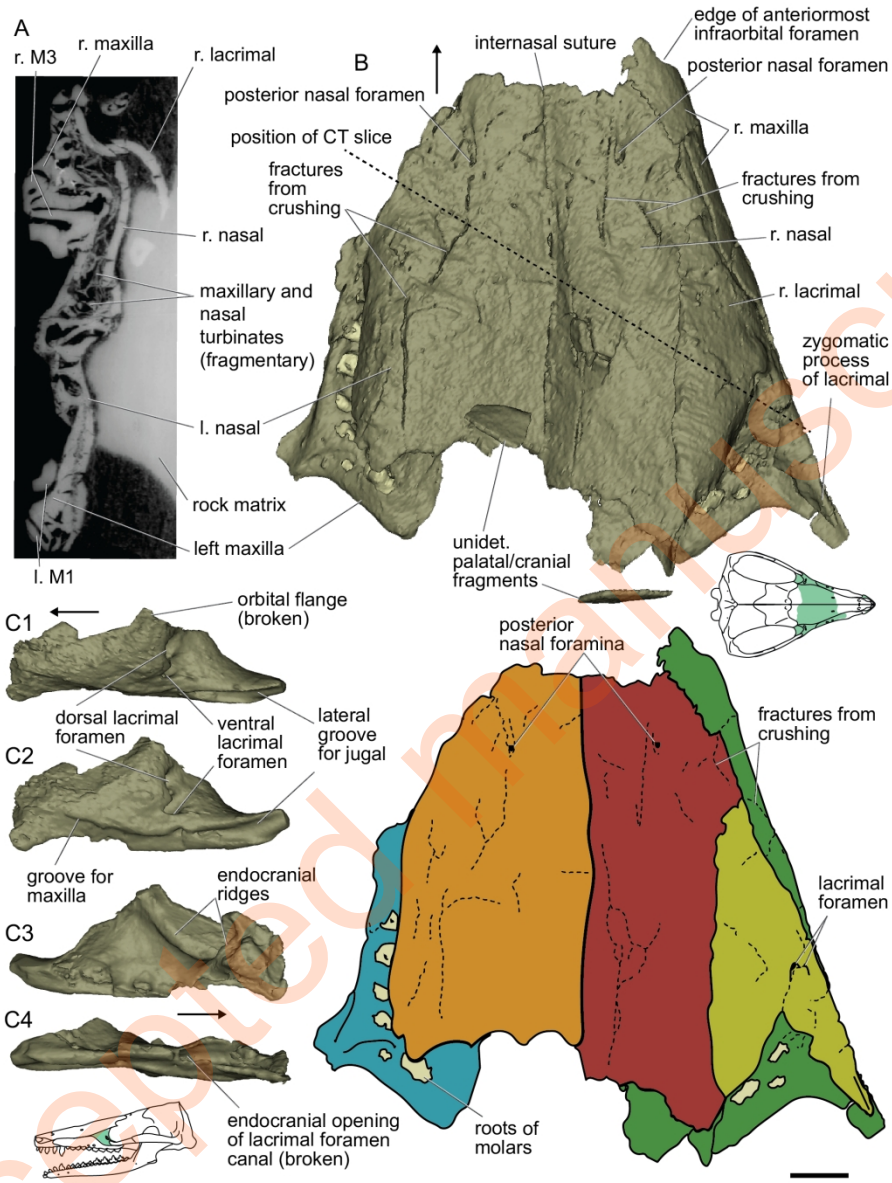

Figure 14: *Borealestes serendipitus* (NMS G.1992.47.121.1) palatal portion of cranium and left lacrimal. A, virtual slice from synchrotron μCT showing cross-section of palate; B, dorsal view with diagrammatic illustration below; C, left lacrimal: C1, dorsal view; C2, left lateral view; C3 medial view; C4, ventral view. Arrows indicate anterior direction. Dark grey areas on diagrammatic illustrations indicate broken surfaces. Scale bar equals 1 mm, scale same throughout.

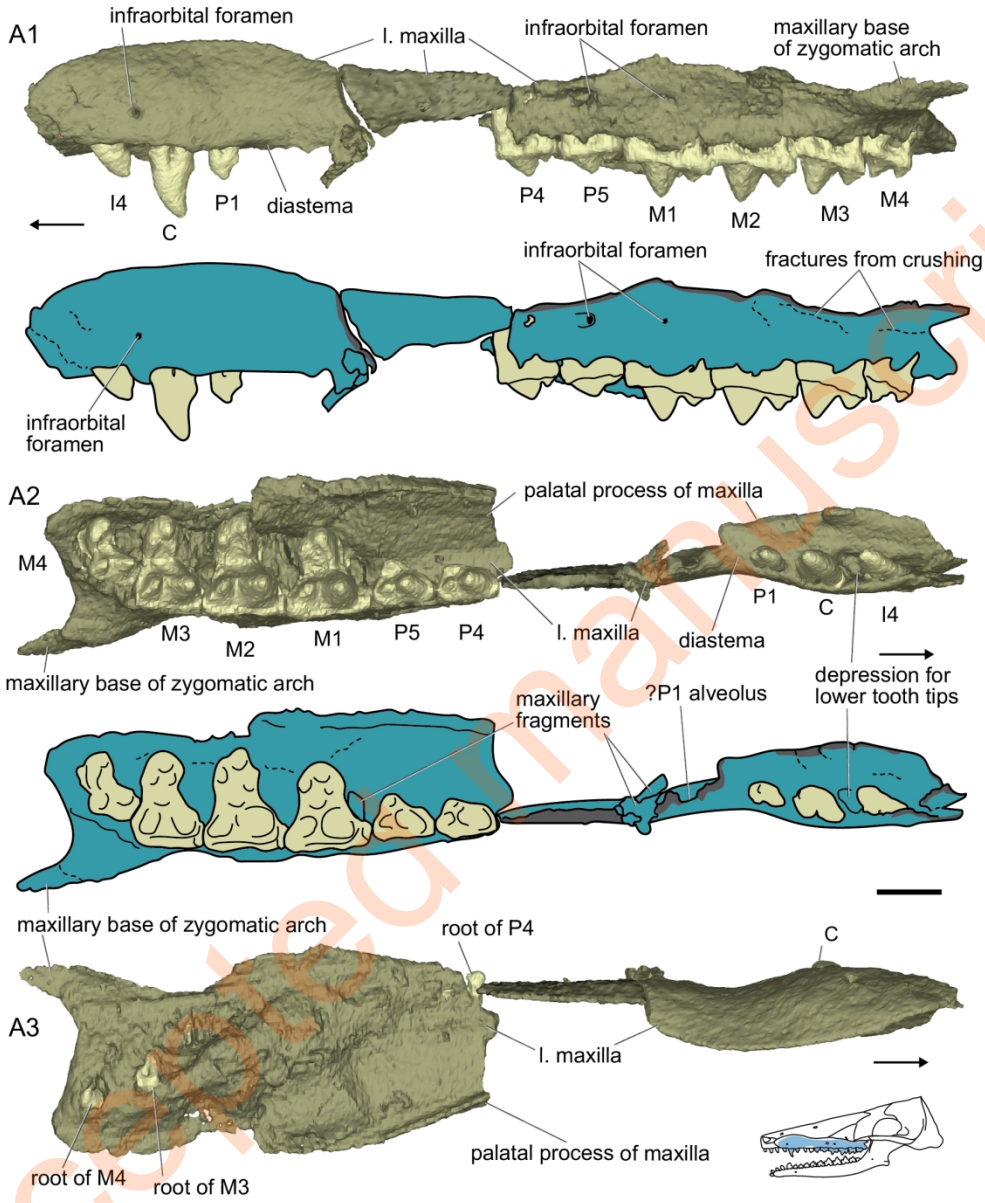

Figure 15: *Borealestes cuillinensis* (holotype, NMS G.2020.4.1.1) left maxilla. A, left maxilla with diagrammatic illustrations: A1, left lateral view; A2, occlusal view; A3, dorsal/endocranial view. Arrows indicate anterior direction. Dark grey areas on diagrammatic illustrations indicate broken surfaces. Scale bar equals 1 mm, scale same throughout.

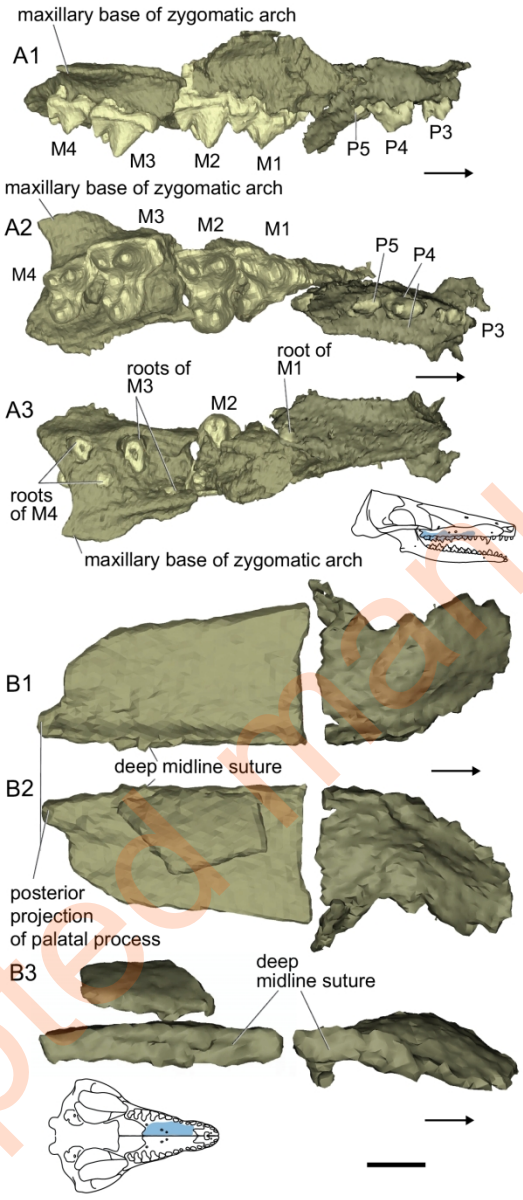

Figure 16: *Borealestes cuillinensis* (holotype NMS G.2020.4.1.1) right maxilla and palatal process. A, posterior portion of right maxilla: A1, right lateral view; A2, occlusal view; A3, dorsal/endocranial view. B, palatal process of right maxilla: B1, dorsal/endocranial view; B2, ventral/palatal view; B3, medial view. Arrows indicate anterior direction. Scale bar equals 1 mm, scale same throughout.

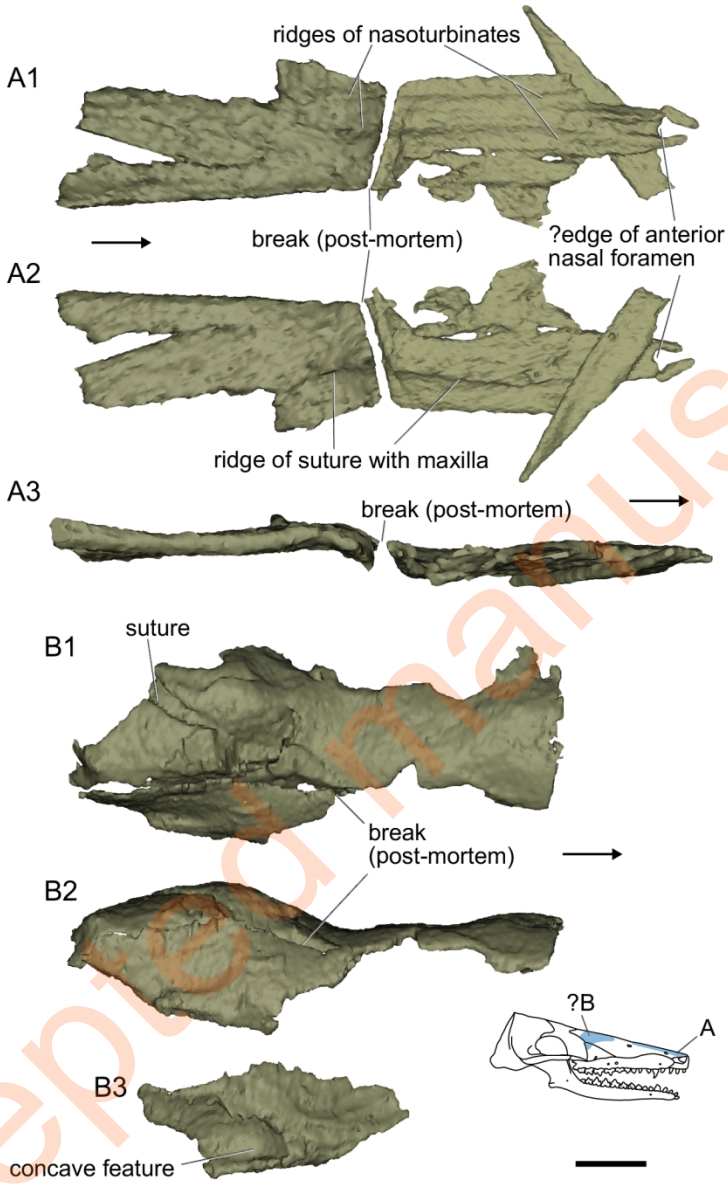

Figure 17: *Borealestes cuillinensis* (holotype, NMS G.2020.4.1.1) nasals and ?lacrimal. A, right nasals: A, ventral/endocranial view; A2, dorsal view; A3, medial view. B, right ?nasal: B1, dorsal view; B2, lateral view; B3, medial/endocranial view. Arrows indicate anterior direction. Scale bar equals 1 mm, scale same throughout.

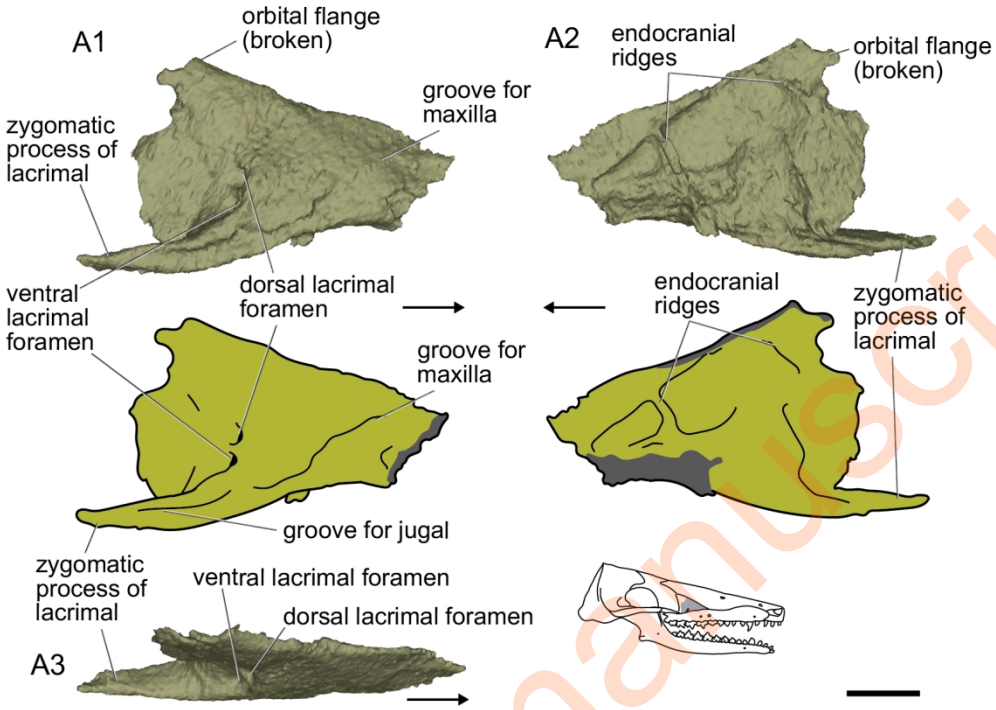

Figure 18: *Borealestes cuillinensis* (holotype, NMS G.2020.4.1.1) right lacrimal and diagrammatic illustrations: A1, right lateral view; C2, endocranial view; C3, dorsal view. Arrows indicate anterior direction. Dark grey areas on diagrammatic illustrations indicate broken surfaces. Scale bar equals 1 mm, scale same throughout.

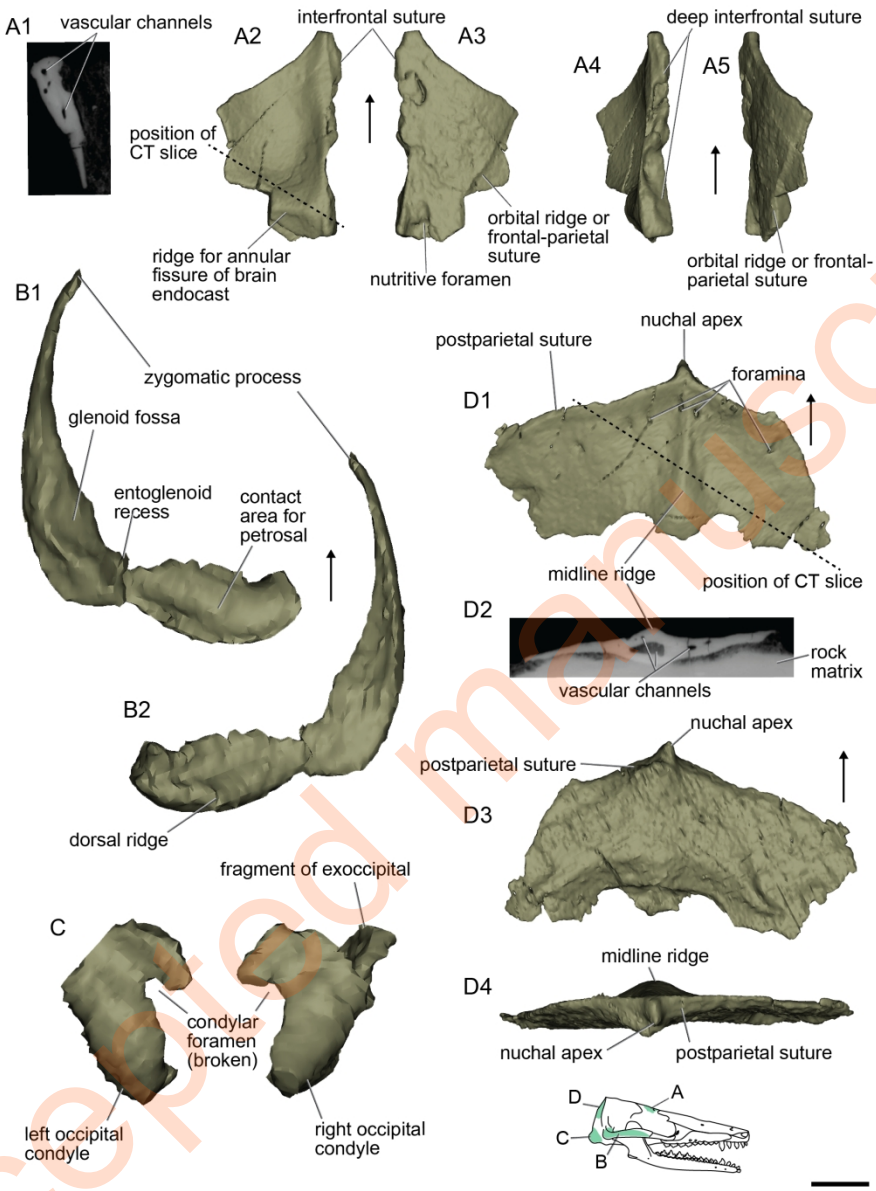

Figure 19: *Borealestes serendipitus* (NMS G.1992.47.121.1) elements of cranium. A, left frontal: A1, synchrotron μCT slice showing cross section through left frontal; A2, ventral view; A3, dorsal view; A4, medial view; A5, left lateral view. B the left squamosal, reconstructed (originally in two misaligned pieces): B1, ventral view; B2, dorsal view; C, the occipital condyles. D, postparietal: D1, posterodorsal view; D2, virtual slice from synchrotron μCT showing cross section through postparietal; D3, anterior/endocranial view; D4, anteroventral view. Arrows indicate anterior direction. Scale bar equals 1 mm, scale same throughout.

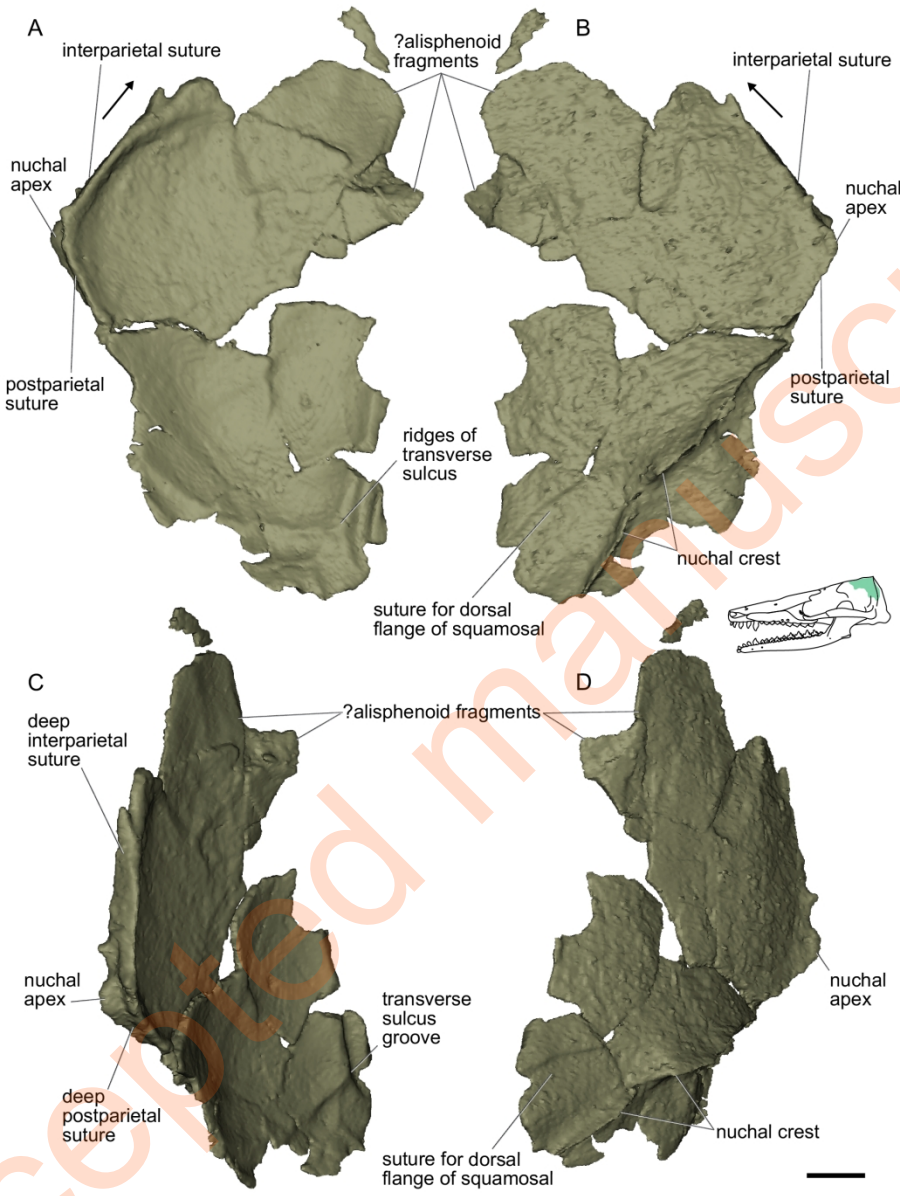

Figure 20: *Borealestes serendipitus* (NMS G.1992.47.121.1) left parietal. A, endocranial/ventral view; B, dorsal view; C, medial view; D, left lateral view. Arrows indicate anterior direction. Scale bar equals 1 mm, scale same throughout.

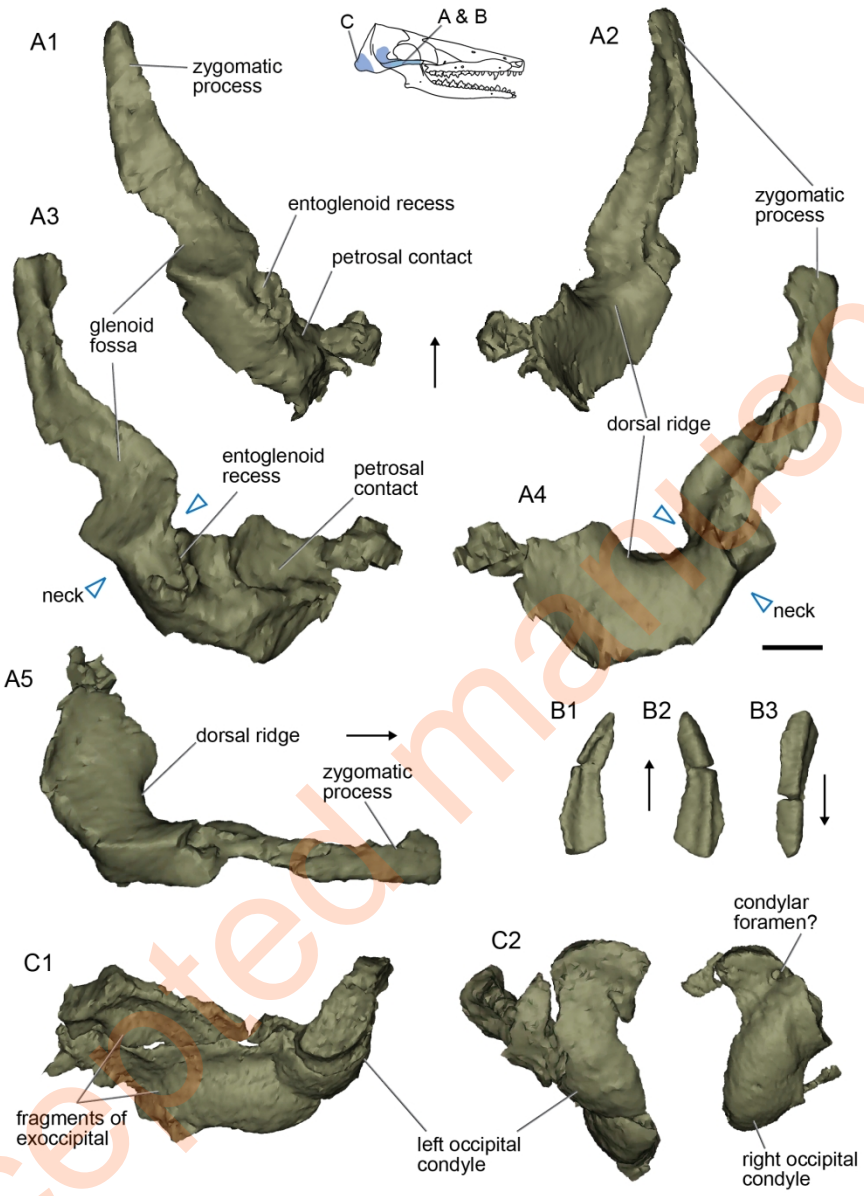

Figure 21: *Borealestes cuillinensis* (holotype, NMS G.2020.4.1.1) squamosal and occipitals. A, the right squamosal: A1, ventral view; A2, dorsal view; A3, medioventral view; A4, laterodorsal view; A5, right lateral view. B, the anterior tip of the left squamosal of (zygomatic process): B1, dorsal view; B2, ventral view; B3, lateral view. C, the occipital condyles: C1, condyles as preserved in specimen; C2, condyles reconstructed. Arrows indicate anterior direction. Scale bar equals 1 mm, scale same throughout.